

# FLUXNET and modelling the global carbon cycle

ANDREW D. FRIEND\*, ALMUT ARNETH†, NANCY Y. KIANG‡, MARK LOMAS§, JÉRÔME OGÉE¶, CHRISTIAN RÖDENBECK||, STEVEN W. RUNNING\*\*, JEAN-DIEGO SANTAREN\*, STEPHEN SITCH††<sup>1</sup>, NICOLAS VIOVY\*, F. IAN WOODWARD§ and SÖNKE ZAEHLE††<sup>2</sup>

\*Laboratoire des Sciences du Climat et de l'Environnement, CEA – Centre de Saclay, Orme des Merisiers LSCE bât. 712, Point courrier 132, F-91191 Gif sur Yvette Cedex, France, †Department of Physical Geography and Ecosystems Analysis (INES), Centre for GeoBiosphere Science, Lund University, Sölvegatan 12, 223, 62 Lund, Sweden, ‡NASA Goddard Institute for Space Studies, 2880 Broadway, New York, NY 10025, USA, §Department of Animal & Plant Sciences, University of Sheffield, Sheffield S10 2TN, UK, ¶EPHYSE (Functional Ecology and Environmental Physics), INRA, BP81, F-33883 Villenave d'Ornon Cedex, France, ||Max-Planck-Institut für Biogeochemie, PO Box 100164, D-07701 Jena, Germany, \*\*School of Forestry, University of Montana, Missoula, MT 59812, USA, ††Potsdam Institut für Klimafolgenforschung (PIK) e.V., Telegrafenberg, PO Box 60 12 03, D-144 12 Potsdam, Germany,

## Abstract

Measurements of the net CO<sub>2</sub> flux between terrestrial ecosystems and the atmosphere using the eddy covariance technique have the potential to underpin our interpretation of regional CO<sub>2</sub> source–sink patterns, CO<sub>2</sub> flux responses to forcings, and predictions of the future terrestrial C balance. Information contained in FLUXNET eddy covariance data has multiple uses for the development and application of global carbon models, including evaluation/validation, calibration, process parameterization, and data assimilation. This paper reviews examples of these uses, compares global estimates of the dynamics of the global carbon cycle, and suggests ways of improving the utility of such data for global carbon modelling.

Net ecosystem exchange of CO<sub>2</sub> (NEE) predicted by different terrestrial biosphere models compares favourably with FLUXNET observations at diurnal and seasonal timescales. However, complete model validation, particularly over the full annual cycle, requires information on the balance between assimilation and decomposition processes, information not readily available for most FLUXNET sites. Site history, when known, can greatly help constrain the model-data comparison.

Flux measurements made over four vegetation types were used to calibrate the land-surface scheme of the Goddard Institute for Space Studies global climate model, significantly improving simulated climate and demonstrating the utility of diurnal FLUXNET data for climate modelling. Land-surface temperatures in many regions cool due to higher canopy conductances and latent heat fluxes, and the spatial distribution of CO<sub>2</sub> uptake provides a significant additional constraint on the realism of simulated surface fluxes.

FLUXNET data are used to calibrate a global production efficiency model (PEM). This model is forced by satellite-measured absorbed radiation and suggests that global net primary production (NPP) increased 6.2% over 1982–1999. Good agreement is found between global trends in NPP estimated by the PEM and a dynamic global vegetation model (DGVM), and between the DGVM and estimates of global NEE derived from a global inversion of atmospheric CO<sub>2</sub> measurements. Combining the PEM, DGVM, and inversion results suggests that CO<sub>2</sub> fertilization is playing a major role in current increases in NPP, with lesser impacts from increasing N deposition and growing season length. Both the PEM and the inversion identify the Amazon basin as a key region for the current net terrestrial CO<sub>2</sub> uptake (i.e. 33% of global NEE), as well as its interannual variability. The

Correspondence: Andrew D. Friend, fax +33 (0)1 69 08 30 73, e-mail: Andrew.Friend@cea.fr

<sup>1</sup>Present address: UK Met Office (JCHMR), Maclean Building, Crowmarsh-Gifford, Wallingford OX10 8BB, UK.

<sup>2</sup>Present address: Laboratoire des Sciences du Climat et de l'Environnement, CEA – Centre de Saclay, Orme des Merisiers LSCE bât. 712, Point courrier 132, F-91191 Gif sur Yvette Cedex, France.

inversion's global NEE estimate of  $-1.2 \text{ Pg [C] yr}^{-1}$  for 1982–1995 is compatible with the PEM- and DGVM-predicted trends in NPP. There is, thus, a convergence in understanding derived from process-based models, remote-sensing-based observations, and inversion of atmospheric data.

Future advances in field measurement techniques, including eddy covariance (particularly concerning the problem of night-time fluxes in dense canopies and of advection or flow distortion over complex terrain), will result in improved constraints on land-atmosphere  $\text{CO}_2$  fluxes and the rigorous attribution of mechanisms to the current terrestrial net  $\text{CO}_2$  uptake and its spatial and temporal heterogeneity. Global ecosystem models play a fundamental role in linking information derived from FLUXNET measurements to atmospheric  $\text{CO}_2$  variability.

A number of recommendations concerning FLUXNET data are made, including a request for more comprehensive site data (particularly historical information), more measurements in undisturbed ecosystems, and the systematic provision of error estimates. The greatest value of current FLUXNET data for global carbon cycle modelling is in evaluating process representations, rather than in providing an unbiased estimate of net  $\text{CO}_2$  exchange.

*Keywords:*  $\text{CO}_2$  exchange, eddy covariance, FLUXNET, global carbon cycle, inversion, model

*Received 12 July 2005; revised version received 26 April 2006 and accepted 1 May 2006*

## Introduction

The equivalent of  $\approx 16\%$  of atmospheric  $\text{CO}_2$  is believed to be cycled through the global land surface each year (Prentice *et al.*, 2001), with terrestrial ecosystems the main driver of global interannual atmospheric  $\text{CO}_2$  variability (e.g. Bousquet *et al.*, 2000; Rödenbeck *et al.*, 2003; Peylin *et al.*, 2005). The eddy covariance technique provides the only direct measurement of net terrestrial ecosystem–atmosphere  $\text{CO}_2$  exchange, and is therefore an indispensable tool for understanding and monitoring the global carbon cycle. As the number of flux observation stations with continuous multiannual observations grows, data from the FLUXNET global network of eddy covariance measurements (Baldocchi *et al.*, 2001) are being used in an increasing number of global carbon cycle modelling studies. This paper reviews a number of these, details their links to FLUXNET, makes some inferences concerning the functioning of the global carbon cycle, and proposes a number of recommendations to augment the utility of eddy covariance data for future global carbon cycle research.

### *Global carbon cycle research*

Despite significant advances over the past decade, major questions remain concerning the role of the terrestrial biosphere in the global carbon cycle. Most notably there is still no consensus on the fate of the approximately 34% (mean 1990s value) of anthropogenic  $\text{CO}_2$  emitted to the atmosphere each year that does not contribute either to the atmospheric burden or enter the oceans (Houghton, 2003). Carbon is believed

to be accumulating in northern mid-latitude terrestrial ecosystems and undisturbed tropical forests, although the magnitude, location, and mechanisms for this accumulation remain subjects of on-going research (Schimel *et al.*, 2001). A likely mechanism for the uptake in mid-latitudes was thought to be the effects of management on forest growth (e.g. fire suppression, agricultural abandonment, and plantation forestry), but careful accounting suggests that significant sinks probably also occur outside of the forest sector (Goodale *et al.*, 2002), possibly due to  $\text{CO}_2$  or N fertilization.

Atmospheric flask measurements reveal large interannual variability in the growth rate of  $\text{CO}_2$  (Conway *et al.*, 1994; Francey *et al.*, 1995; Keeling *et al.*, 1995) and, when combined with atmospheric tracer transport models to infer the pattern of sources and sinks by inversion, suggest strong regional patterns in net  $\text{CO}_2$  fluxes (e.g. Rödenbeck *et al.*, 2003). However, the inversion technique cannot directly attribute these signals to mechanisms.

Simulations using six dynamic global vegetation models (DGVMs) revealed major uncertainties in the terrestrial carbon balance response to future climate and  $\text{CO}_2$  change (Cramer *et al.*, 2001). Because of the importance of  $\text{CO}_2$  as a radiatively active gas, our limited understanding of terrestrial carbon cycling translates into a major source of uncertainty for predictions of future climate change (e.g. Friedlingstein *et al.*, 2003; Jones *et al.*, 2003).

### *Eddy covariance data*

Multiannual eddy covariance data are now available for a wide range of ecosystem types, and therefore have the potential to significantly improve our understanding of

controls on land-atmosphere CO<sub>2</sub> exchange (Baldocchi *et al.*, 2001). These data consist of the vertical flux densities of CO<sub>2</sub>, latent heat, and sensible heat measured using sensors placed above the canopy, together with meteorological conditions. The fluxes are typically integrated to half-hourly or hourly means (Aubinet *et al.*, 2000). Data gaps, caused by sensor failures or unsuitable micrometeorological conditions (e.g. heavy rainfall) are unavoidable (Falge *et al.*, 2001), but these can be filled using a variety of techniques to produce a continuous time series. Underevaluation of night-time CO<sub>2</sub> fluxes due to stable atmospheric conditions (Kruijt *et al.*, 2004), and problems with closing the energy budget (Wilson *et al.*, 2002), suggest caution in the uncritical use of data integrated over a diurnal cycle or longer, when the measured fluxes may not be equal to the ecosystem fluxes.

#### Uses for FLUXNET data in global carbon modelling

FLUXNET data are important sources of information for the advancement of models used to study the global carbon cycle. These data are most commonly used to evaluate/validate and/or calibrate ecosystem models for particular ecosystem types. More recently, they have been used in parameter estimation and optimization procedures (e.g. Knorr & Kattge, 2005), and are being considered for incorporation into data assimilation systems (Raupach *et al.*, 2005). This paper discusses a number of these applications.

The linkages between FLUXNET data and the different studies presented in this paper, and their temporal/spatial contexts, are shown in Fig. 1. Reviews of model evaluation/validation exercises are taken from three DGVMs: the Sheffield dynamic global vegetation model (SDGVM), the Lund-Potsdam-Jena (LPJ) model, and ORCHIDEE. DGVMs are designed to predict the transient dynamics of vegetation (and in most cases soil organic matter) at a range of temporal (minutes to centuries) and spatial (typically half-degree to global) scales. They are based on the calculation of the flux of C into the vegetation and its dependence on environmental conditions, and can therefore be tested directly using FLUXNET data. They typically contain a number of parameters that are rather poorly constrained, and an example is given of how FLUXNET data can be used directly to optimize various key model parameters. Examples are also reviewed for how FLUXNET data are used to calibrate global satellite-driven (production efficiency model (PEM)) and climate (Goddard Institute for Space Studies (GISS) global climate model (GCM)) models. Finally, an atmospheric inversion modelling study is presented and the potential future application of FLUXNET data combined with flask measurements for better constraining the spatial and temporal dynamics of the global carbon cycle is discussed. The following sections, apart from the final one on atmospheric inversion, focus on key findings that have arisen directly from the use of FLUXNET data.

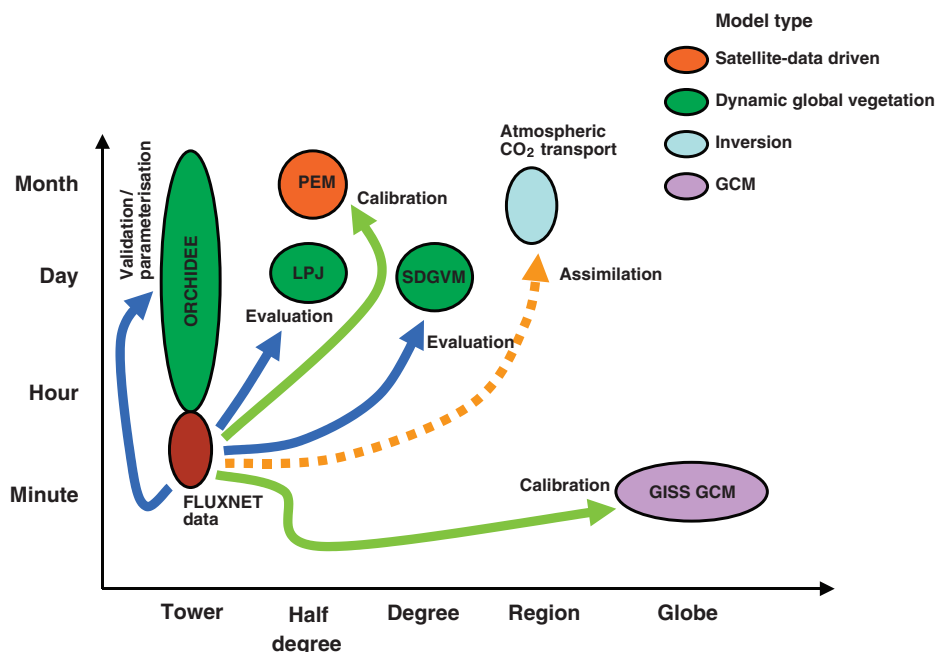


Fig. 1 Relationships between FLUXNET data and the modelling studies discussed in this paper. Scales show the main temporal and spatial emphases. Solid arrows indicate transfer of information. Dotted arrow indicates potential future application.

## Applications of FLUXNET data in global carbon cycle modelling

### Importance of site history for model-data comparisons

In common with other models of its type, the SDGVM predicts global vegetation structure and dynamics from climate, atmospheric CO<sub>2</sub> concentration, and soil texture (Woodward *et al.*, 1995; Woodward & Lomas, 2004). FLUXNET data have the potential to strongly constrain DGVM predictions of CO<sub>2</sub> fluxes. The SDGVM was evaluated by comparing mean output for 1990–1995 from a global simulation (Woodward & Lomas, 2004) against available FLUXNET data (generally collected 1995–2000). Comparisons were made with modelled mean annual leaf area index (LAI), net ecosystem-atmosphere CO<sub>2</sub> exchange (NEE), total canopy N, gross primary production (GPP), respiration, and canopy height in the 1° pixel containing each FLUXNET tower.

Simulated mean annual LAI is in good agreement with the observations (Fig. 2a). However, comparison between simulated and measured mean annual NEE indicates an underprediction at sites with high measured net CO<sub>2</sub> uptake (Fig. 2b). The model was allowed to reach equilibrium and then forced with observed interannual climate variability over 1901–1995. Clearly this forcing is not sufficient to create the large observed disequilibrium between CO<sub>2</sub> uptake and loss at many FLUXNET sites. It seems that exogenous disturbances not included in the simulations need to be invoked, a suspicion confirmed by highlighting those sites known to have been planted or managed in the recent past (Fig. 2b). Inclusion of these disturbances in the simulations would allow a more critical evaluation of the model's performance.

The possible role of disturbance in explaining the difference between modelled and measured mean annual NEE was further investigated at one of the sites with the greatest mismatch, Aberfeldy in Scotland. This FLUXNET site is a Sitka spruce (*Picea sitchensis* (Bong.) Carr.) plantation, whereas the model predicts a mixed evergreen/deciduous forest, with NEE about half that observed. Mean annual GPP is also predicted to be much lower than the value estimated from the flux measurements (from extrapolation of night-time fluxes to estimate respiration), and, therefore, the mismatch cannot be only due to (dis)equilibrium. The plantation

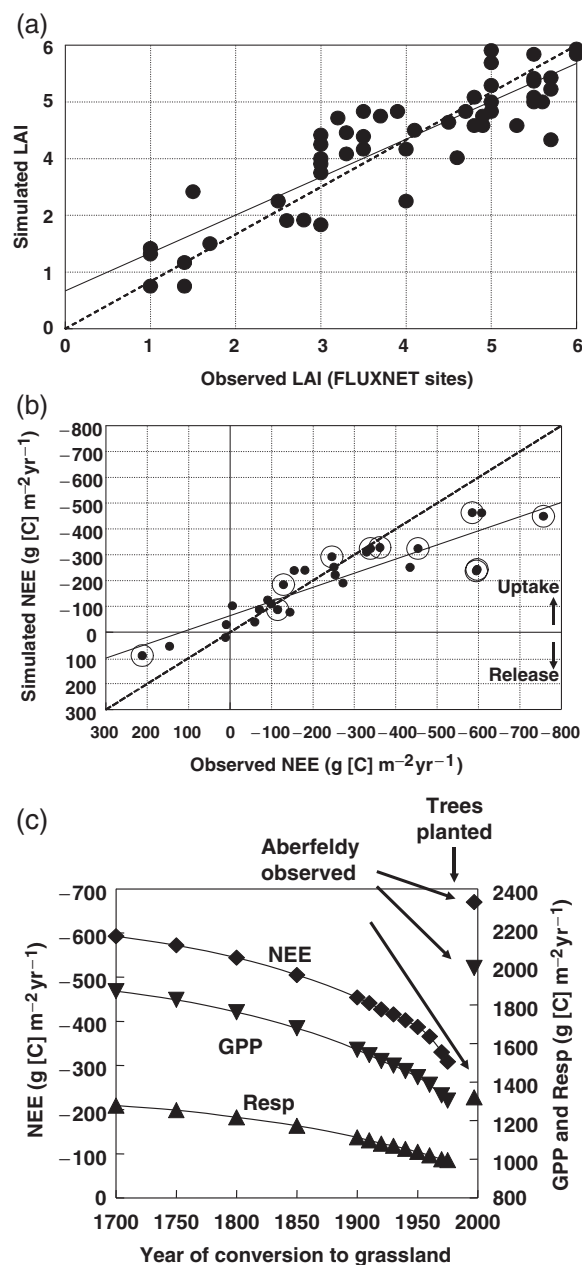


**Fig. 2** Simulation results obtained using the Sheffield dynamic global vegetation model compared with FLUXNET observations, from Woodward & Lomas (2004). Model estimate is the 1990–1995 mean prediction over the 1° pixel containing each flux tower. (a) Regression of mean annual simulated LAI against observations. Broken line, 1:1 relationship; continuous line, regression equation  $y = 0.8x + 0.8$ ;  $r^2 = 0.8$ ,  $n = 52$ . (b) Regression of mean annual simulated net ecosystem exchange of CO<sub>2</sub> (NEE) against observations (inverted scales). Broken line, 1:1 relationship; continuous line, regression equation  $y = 0.55x - 63.87$ ;  $r^2 = 0.8$ ,  $n = 28$ . Double circles indicate sites with forest age  $\leq 50$  years. (c) Predicted and observed mean annual CO<sub>2</sub> fluxes at a site in Scotland (56.6°N; 3.8°E). This site was planted with evergreen needle-leaved forest in 1980. Diamonds with line: simulated NEE; single diamond: 1997 observed NEE; inverted triangles with line: simulated gross primary production (GPP); single inverted triangle: 1997 observed GPP; triangles with line: simulated ecosystem respiration; single triangle: 1997 observed ecosystem respiration. NEE plotted on inverted scale.

was established in 1980 on an area of previous sheep grazing, and additional simulations were performed in which trees were inhibited from establishing for varying lengths of time before the actual planting date (Fig. 2c). Interestingly, predicted NEE and GPP approach the observed values as the time under pasture increases. Tree GPP increases with length of time under pasture because of the greater subsequent availability of soil N, built up over years of grass growth and litter production. This example clearly shows the critical role of site history for comparison of modelled mean annual NEE with eddy covariance data.

It is also evident that rigorous model validation requires knowledge of the observational errors, but these are difficult to obtain for flux measurements (Dore *et al.*, 2003). Error estimates across different sites range between  $\pm 30$  and  $\pm 180 \text{ g[C] m}^{-2} \text{ yr}^{-1}$ , which are of the same order as the model-data difference (Woodward & Lomas, 2004), and may be even higher at some locations (Kruijt *et al.*, 2004). Sources of these errors include instrument calibration, data gaps, and atmospheric processes that reduce the correspondence between the measured flux and the ecosystem flux (e.g. advection or high atmospheric stability). In terms of cumulative (e.g. annual) NEE, random and fully systematic errors are generally of lesser concern than selective systematic errors, because the latter exist only for part of the daily  $\text{CO}_2$  cycle when fluxes are either positive or negative (Moncrieff *et al.*, 1996). The model also has error in relation to the measured ecosystem through the assumption of natural (potential) vegetation with long-term equilibrium between fixation and respiration, system attributes unlikely to be true at most eddy flux sites. Rigorous incorporation of these error terms into model-data comparisons remains a subject of on-going research (Hollinger & Richardson, 2005).

#### Importance of forest age structure and forest management

Like the SDGVM, the LPJ DGVM (Sitch *et al.*, 2003) is a global model of vegetation distribution and dynamics. LPJ was used to investigate the observed latitudinal gradient in NEE deduced from analysis of data from 15 European FLUXNET sites and reported by Valentini *et al.* (2000). Observations indicated that most sites were gaining C, with a significant increase in net uptake with decreasing latitude (Fig. 3a). In the original analysis, data of  $\approx 1$  year per site were presented but the latitudinal trend persists over longer time periods. GPP appeared to be largely independent of latitude, leading to the conclusion that the gradient results from relatively higher respiration at more northerly sites.

The ability of the LPJ model to simulate this gradient was investigated by running the model with the ob-

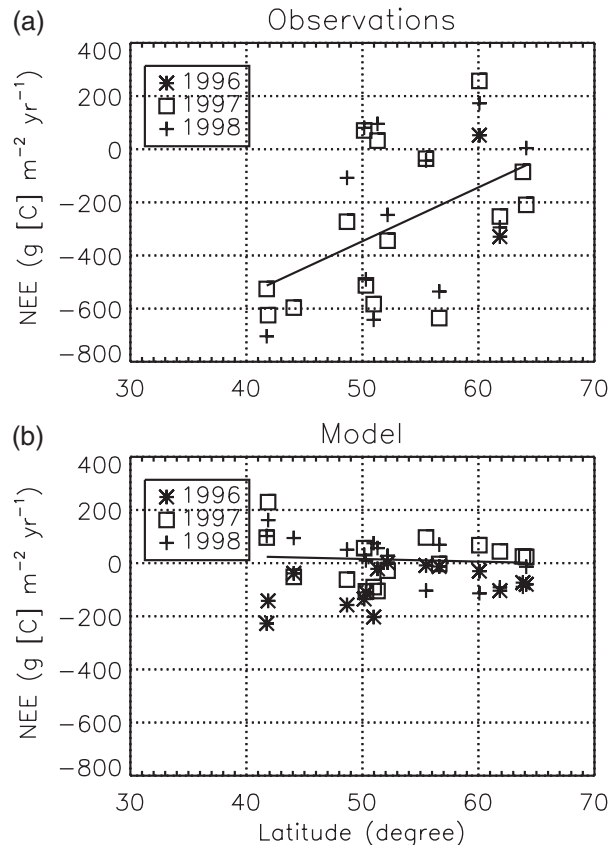


**Fig. 3** Observed (a) and modelled (b) latitudinal gradient in mean annual net ecosystem exchange of  $\text{CO}_2$  (NEE) (i.e. heterotrophic respiration – net primary production) at 15 European FLUXNET sites. Model is the Lund–Potsdam–Jena (LPJ) model. Lines are linear regressions to data (a) and model (b) for 1997.

served climate at each FLUXNET site and ensuring that model and site plant functional type (PFT) agreed. The latter is an important aspect as not all sites contained the potential natural vegetation. Before forcing by the actual climate, the model was run to C equilibrium at each site using a long-term mean climatology as with the SDGVM. Although agreement between simulated and modelled monthly NEE is rather good (with some notable exceptions), the model does not reproduce the observed latitudinal gradient in NEE, but rather predicts a much smaller, annually varying gradient (Fig. 3b). In particular, the large net sink of  $>400 \text{ g[C] m}^{-2} \text{ yr}^{-1}$  reported for the more southerly sites is not reproduced by the model in any year. Moreover, the spread of NEE at a given latitude is noticeably smaller in the simulation results.

It is important to know if these model-data mismatches are caused by a basic inadequacy of the model or specific site characteristics such as their

management history. Unfortunately, it is difficult to obtain accurate and detailed site history information for many of the sites. However, European settlement history suggests that sites in the southern and central parts of the continent were influenced by intensive use by humans for >2000 years. Northern forests have probably only experienced large-scale management for a few tree generations and fewer changes in management practices. Long-term removal of woody stem biomass and/or the presence of animal grazing in the forest would be expected to affect soil C input and, therefore, respiration rates, as well as mean tree growth rates.

To test this in a model context, additional simulations were performed with LPJ to examine NEE sensitivity to different management effects. For example, the simulation at the northern Scots pine (*Pinus sylvestris* L.) site, Hyytiälä, Finland (61°85'N) was repeated, but with an imposed aboveground wood harvest in 1966, as actually occurred. This had the effect of somewhat reducing winter respiration rates and therefore producing a slightly better fit to the data. However, incorporating one harvest cycle was not sufficient to reproduce the effects of probable longer-term human impacts, particularly in an aggregated model such as LPJ. Site history clearly has an important impact on annual and longer-term NEE, although it does not seem to play a large role in seasonal variability.

At the European scale, uncertainty in model parameters without accounting for site history is not sufficient to explain the discrepancy between model and observations, based on both forest inventories and FLUXNET data (Fig. 4; Zaehle *et al.*, 2005). After evaluation of stand-scale growth patterns, Zaehle *et al.* (2006) incorporated forest age structure and a generic representation of forest management in even-aged stands into LPJ. With this advanced model, Zaehle *et al.* (2006) studied the effects of changing land use, wood demand, and climate on European forest ecosystems over 1948–2000. They were able to reproduce the present-day age structure and ratio of removals to increment in European forests, as well as model present-day C sequestration in vegetation in agreement with independent forest inventory-based estimates. NEE based on the improved model is within the range of uncertainty in the observations when land-use change (LU) and wood demand change (FM) are considered (Fig. 4). Nevertheless, simulated C uptake remains lower than data-based estimates, possibly because the simulations do not take into account the effects of soil degradation resulting from past land-management practices. Indeed, uncertainty in the historical soil C stock is critical to our ability to determine the present-day NEE in European forests (Janssens *et al.*, 2003).

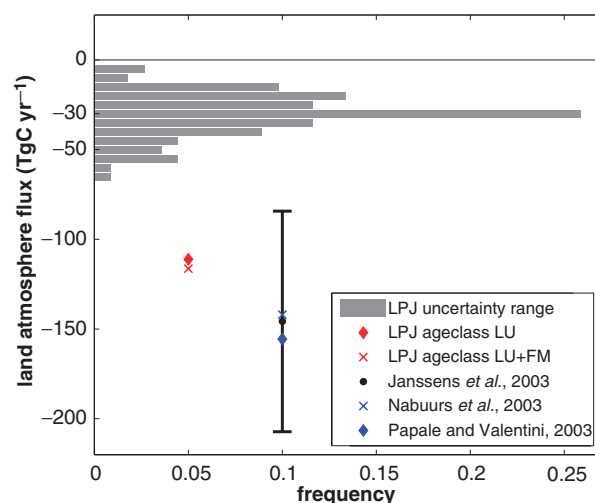


Fig. 4 Modelled and data-based estimates of net ecosystem exchange of CO<sub>2</sub> over the European forest area (1.51 Mio km<sup>2</sup>) in the 1990s. The uncertainty range describes the parameter-based uncertainty of the standard version of Lund–Potsdam–Jena (LPJ), whereas ‘LPJ ageclass’ refers to the extended version of LPJ that explicitly accounts for forest age structure, and the effects of land-use change (LU) and wood demand changes (FM). Nabuurs *et al.* (2003) used forest resource statistics to derive the carbon uptake in forests, whereas Papale and Valentini (2003) relied on data from European FLUXNET sites.

#### Validating modelled diurnal and seasonal fluxes from a DGVM

Like the SDGVM and LPJ, ORCHIDEE is a DGVM, but differs somewhat in that it is designed to be coupled to models of the global atmospheric circulation. ORCHIDEE consists of three linked submodels: SECHIBA computes land-atmosphere energy and water exchanges on a 30 min time step; vegetation dynamics parameterizations, such as sapling establishment, mortality, competition for light, and PFT climate envelopes, are taken from LPJ (Sitch *et al.*, 2003); and phenology and C fluxes such as photosynthesis, respiration, and allocation are treated by the submodel STOMATE. A full description of ORCHIDEE is given by Krinner *et al.* (2005).

A series of site-level simulations were performed with ORCHIDEE and compared with FLUXNET data in order to evaluate the model’s ability to predict biosphere–atmosphere fluxes. Thirty-one sites were chosen across a wide range of PFTs with long-term and more-or-less continuous measured fluxes and forcing. Only sites representative of tropical drought deciduous forest (e.g. Miombo woodlands) were unavailable. Unfortunately, some sites only had available data for the growing season, and many others had gaps

in the climate data, which had to be filled to enable model simulations. The latter was achieved using data from nearby weather stations and the ECMWF ERA15 1° reanalysis product (see Krinner *et al.*, 2005 for details).

The model was compared with measured fluxes of CO<sub>2</sub>, moisture, sensible heat, and net radiation at diurnal and seasonal timescales, using prescribed vegetation type; LAI, photosynthetic capacity, and soil C were predicted. Lack of information concerning site history means that initialization of the model is problematical. A spin-up was performed with recycled observed site climate until decomposition was in equilibrium with plant production, as discussed above for simulations with the SDGVM and LPJ models. However, a direct comparison between the equilibrium model predictions and site data would not then be a good test of the model as the data tend to show a net long-term sink, most likely due to management history as discussed above (see also Law *et al.*, 2002). Therefore, to better evaluate the model's ability to represent diurnal and seasonal variability in C fluxes, and in contrast to the model evaluations described above, the output was corrected for the observed long-term net flux at each site, forcing model and data to have the same annual NEE (Krinner *et al.*, 2005).

ORCHIDEE predictions of the mean June–July–August (JJA) diurnal cycle are compared with observations averaged for each PFT in Fig. 5, with good overall agreement. Some issues revealed by these comparisons include the model's simulation of albedo at crop sites during the winter (the model does not account for harvest), a general overestimate of sensible heat fluxes (probably due to the use of a bulk energy budget for vegetation and soil), insufficient stomatal control on afternoon latent heat fluxes at Mediterranean sites (i.e. 'temperate EBF'), an underprediction of the NEE amplitude at needle-leaved forest sites (ENF), and an over-prediction at broad-leaved forest sites (DBF) (possibly due to the relatively simple canopy integration of photosynthesis). However, the model succeeds in capturing the main differences between the PFTs in terms of peak fluxes.

Seasonal predictions are compared with observations in Fig. 6, and again there is good overall agreement. The most notable area of disagreement is the general overestimation of the sensible heat flux. The exact reasons for this are not known, but are the subject of on-going investigations. ORCHIDEE tends to overestimate soil drought towards the end of the summer at Mediterranean sites, resulting in lower predicted latent heat flux (LE) and NEE at this time than observed. Mismatches for the boreal deciduous broad-leaved tree (DBF) PFT are likely due to problems with the precipitation forcing

data. Overall, the seasonal phasing of each flux is predicted well, suggesting that leaf out and leaf fall are simulated realistically.

*Parameter optimizing in a DGVM: strong constraints for photosynthesis, weak constraints for respiration*

Ideally, parameters and initial conditions for ecosystem models are estimated from process studies. However, most parameters and processes cannot be observed directly and observed parameters must be scaled up from the measurement scale to the eddy covariance footprint scale. These issues have been successfully addressed using inverse modelling. Maximum likelihood methods (Tarantola, 1987; Press *et al.*, 1992) can provide estimates of model parameters from eddy covariance flux data. These methods can be gradient-based (Wang *et al.*, 2001; Reichstein *et al.*, 2003), or based on Monte-Carlo (MC) frameworks (Franks & Bevan, 1997; Gupta *et al.*, 1999; Schulz *et al.*, 2001). These methods search to find parameter sets that yield the best match between data and model. Three principal factors can explain data-model mismatch: structural deficiencies of the model, data error (e.g. gaps or outliers), and/or parameter misspecification. Optimization can decrease only the latter source of error, although it can also highlight which model processes may need to be modified.

Parameters are not equally constrained by data because the information content of the data depends on the process and because model output sensitivity can vary between parameters. Therefore, it is important to assess the information that the optimization methods can transfer into the retrieved parameters in order to assign confidence levels to inferred values. Very efficient techniques using MC frameworks allow complete determination of the probability distribution of the inverted parameters (Schulz *et al.*, 2001). Other, cruder, but less computationally expensive techniques, derive standard deviations by assuming that data and model errors are distributed normally (Kaminski *et al.*, 2002). For both types of methods, knowledge of the inherent flux measurement uncertainty is necessary to correctly determine the confidence intervals of model parameter estimates (Hollinger & Richardson, 2005).

A number of parameters in the ORCHIDEE model were optimized against measurements of CO<sub>2</sub>, latent heat, and sensible heat fluxes, as well as net radiation, over a pine forest near Bordeaux, France. A Bayesian inverse approach (Tarantola, 1987) was designed to estimate the mean value and the uncertainty of 12 parameters related to C and energy exchanges. Assimilating three consecutive weeks of data during the 1997 growing season results in a set of optimized parameters

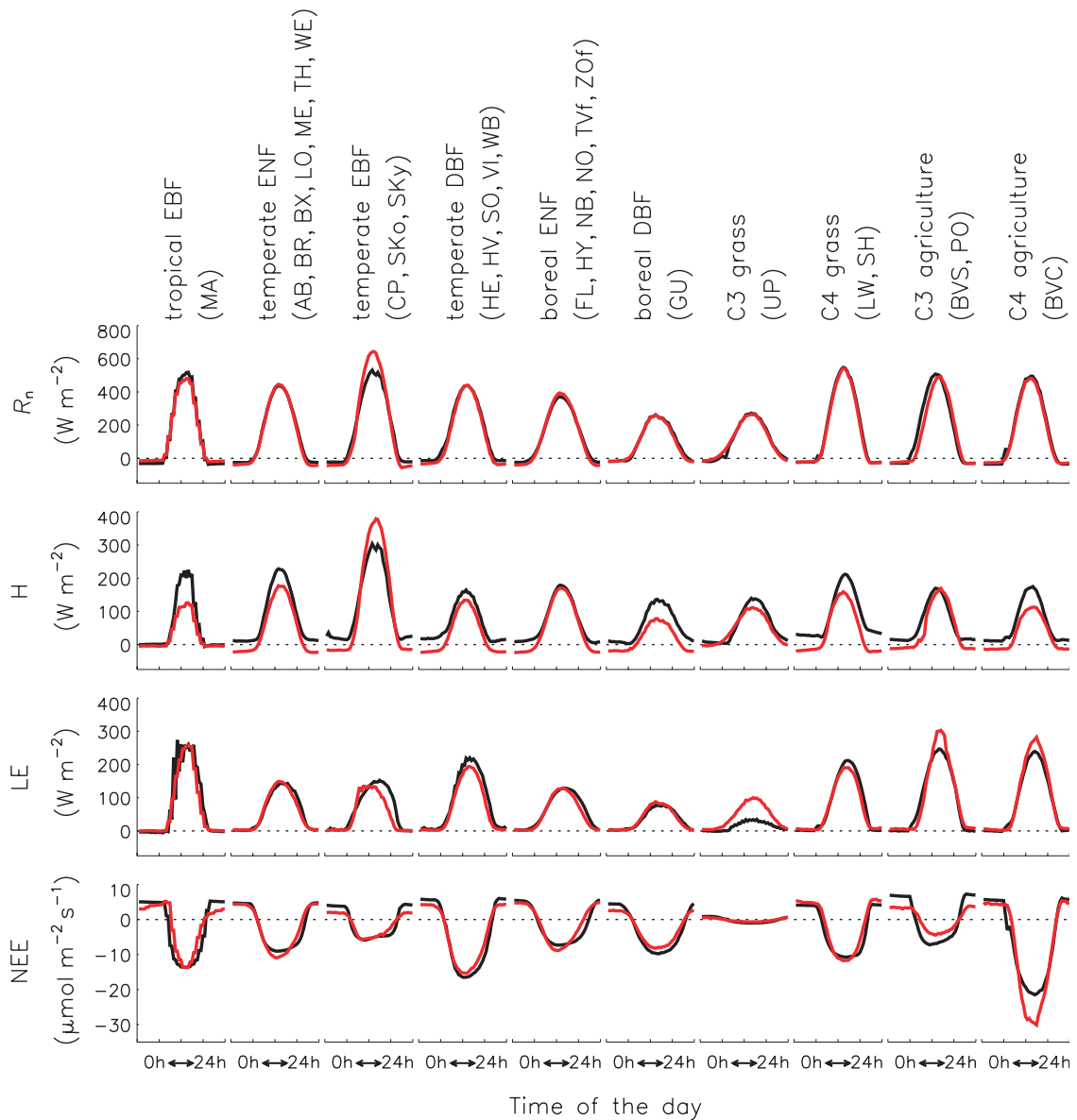


**Fig. 5** Measured FLUXNET (red) and ORCHIDEE simulated (black) JJA mean diurnal cycles for each flux and each plant functional type. Panels show net radiation ( $R_n$ ), sensible heat flux ( $H$ ), latent heat flux ( $LE$ ), and net CO<sub>2</sub> flux ( $NEE$ ). Values are bin-averaged. Figure redrawn from Krinner *et al.* (2005), which gives details of the sites listed in the figure as letter codes.

(Fig. 7) which greatly improve the fit to the observed diurnal cycle, except for the sensible heat flux at night. To improve the model, four parameters ( $K_{vmax}$ ,  $\beta$ ,  $f_{stress}$  and  $K_{Csoil}$ ; see Fig. 7 legend for definitions) are robustly inferred from the flux data. That is, the *a posteriori* uncertainties are very small compared with parameters that are poorly constrained (i.e.  $K_{MR}$ ,  $Q_{MR}$ ,  $K_{GR}$ ,  $K_{HR}$ ,  $K_{Ra}$  and  $K_{Z0}$ ). It is notable that the optimization against the CO<sub>2</sub> flux does not allow the constraint of respiration parameters. A third class of parameters have nonregular behaviour (i.e. are optimized beyond *a priori* limits), that may highlight structural deficiencies of the model.

For example, the parameter scaling the surface albedo,  $K_{alb}$ , is set to its lower *a priori* bound, yielding a spurious value (i.e. 0.1) for a pine forest, possibly due to model deficiencies related to the energy balance calculation (the model does not simulate the temperature gradient inversion that occurs during the night within the canopy). Also, the  $Q_{10}$  parameter is set to unity (normalized value of 0.5), thus removing the temperature dependency of the heterotrophic respiration. This probably indicates that a  $Q_{10}$  relationship, which is valid at seasonal time scales (Raich & Schlesinger, 1992), is not valid diurnally (at least for this model).

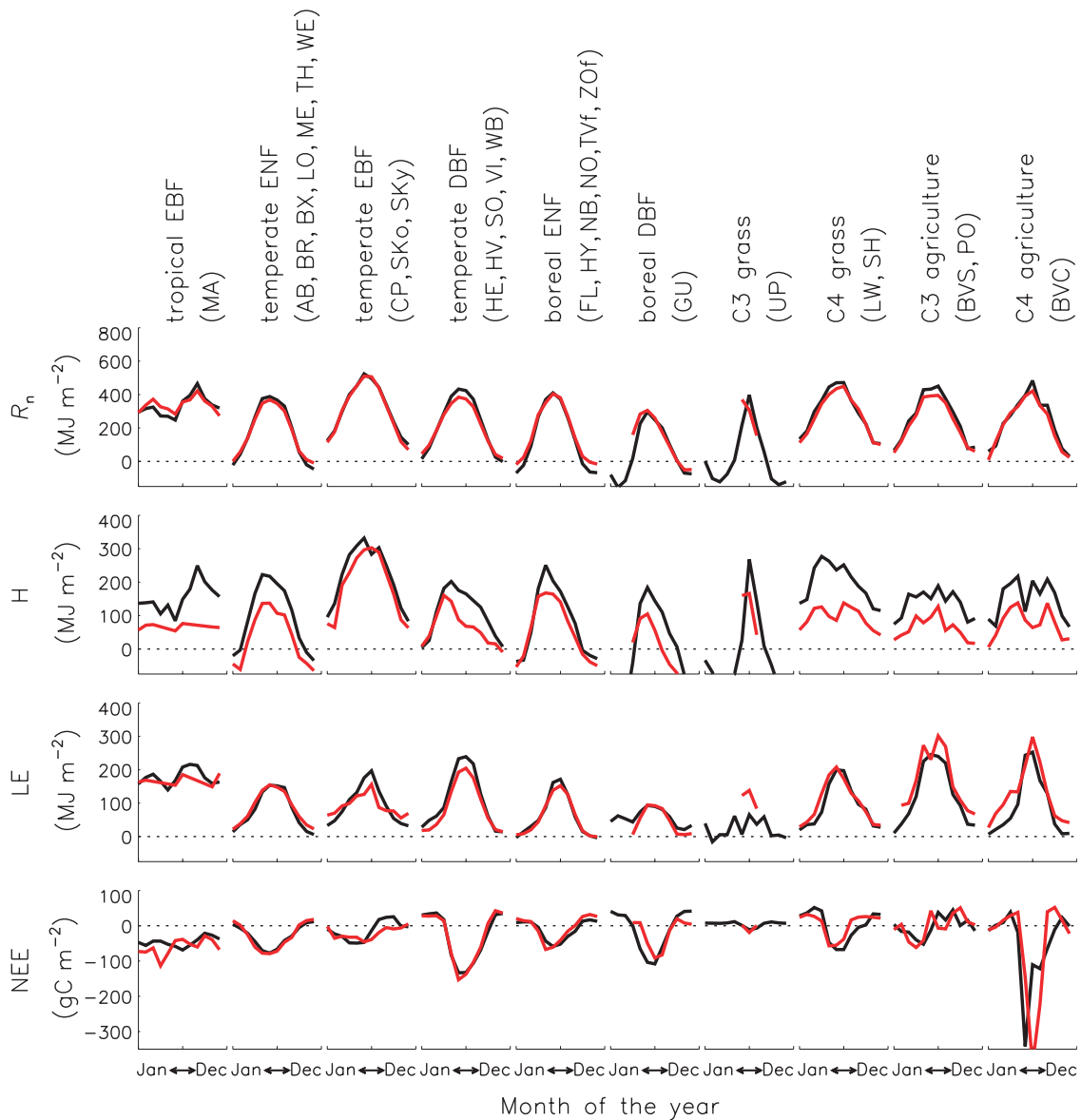


Fig. 6 As Fig. 5, but mean seasonal cycles.

Some parameter values, although well constrained, could be spurious. Indeed, if the underlying model is wrong or incomplete, we could have a good fit to the data but with misleading inferred values. Also, the optimized values could be strongly biased by data outliers. Independent *in situ* measurements can then be useful checks of the optimization consistency. In Fig. 8, the optimized carboxylation rates  $V_{\text{cmax}}$  and  $V_{\text{jmax}}$  (optimized via the multiplier  $K_{\text{vmax}}$ ) are compared with independent leaf scale measurements (Porté & Loustau, 1998). For young and old needles, optimized age-related variations of  $V_{\text{cmax}}$  and  $V_{\text{jmax}}$  (Ishida *et al.*, 1999) are closer to the observations than the *a priori* curves.

In conclusion, optimization against flux measurements allows some parameters to be determined (such

as the leaf carboxylation efficiency and the photosynthesis/conductance ratio) and model deficiencies highlighted. The method also allows the assessment of the information content of eddy covariance data, such as its inability to determine a value for the  $Q_{10}$  of soil decomposition on diurnal timescales.

#### *Improving climate simulations through land-surface model calibration*

Until recently, the NASA GISS GCM land-surface scheme contained a relatively simple treatment of vegetation processes, with no representation of C fluxes (Rosenzweig & Abramopoulos, 1997). This earlier version of the GCM treated bulk canopy conductance using

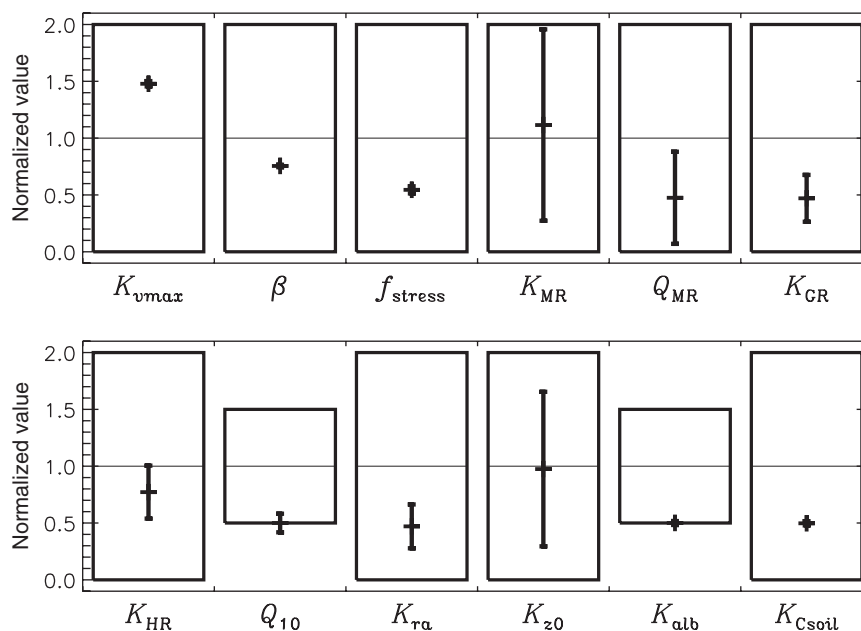


**Fig. 7** ORCHIDEE parameter estimates and errors. Optimized values are normalized by the *a priori* estimate (horizontal line in the boxes centered at normalized value of 1). The box's half height equals the normalized *a priori* uncertainty. Within each box, the parameters and errors retrieved from 3 weeks of data at the Bray, France, forest (days 195–216 of 1997) are given. Among the optimized parameters, 'biophysical' parameters acting on photosynthesis and transpiration ( $K_{vmax}$ , carboxylation maximum rate multiplier;  $\beta$ , slope of stomatal conductance;  $f_{stress}$ , soil water stress dependency of the canopy stomatal conductance slope), surface energy budget ( $K_{alb}$ , surface albedo multiplier;  $K_{Csoil}$ , soil heat capacity multiplier), and turbulent transfer scalars ( $K_{ra}$ , aerodynamic resistance multiplier;  $K_{z0}$ , roughness length) can be distinguished from 'biological' parameters ( $K_{MR}$ , rate of plant maintenance respiration constant;  $K_{GR}$ , rate of plant growth respiration constant;  $K_{HR}$ , rate of microbial respiration constant;  $Q_{MR}$ , temperature dependency of maintenance respiration;  $Q_{10}$ , temperature dependency of microbial respiration) acting on respiration terms.

a simple empirical function of incident shortwave radiation, canopy temperature, soil moisture, LAI, and minimum leaf stomatal resistance (Rosenzweig & Abramopoulos, 1997). This deficiency has been addressed through the development of a new plant canopy model that additionally simulates canopy conductance responses to moisture and the net canopy  $CO_2$  flux (Friend & Kiang, 2005; Schmidt *et al.*, 2006).

The new model uses process-based representations of photosynthesis and the within-canopy variability in physiological capacity and light environment. A semi-empirical stomatal model is included, and quantities are expressed on a photosynthetic N basis, allowing mechanistic scaling to the leaf, canopy, and different vegetation types. A full description of the model is given by Friend & Kiang (2005).

The new GISS GCM vegetation canopy model was tested by comparing predicted canopy conductance and  $CO_2$  fluxes against 10 days of measurements at four FLUXNET sites with different vegetation types. A number of quantities were first inferred from the measured fluxes and meteorological conditions to more precisely evaluate the model (see Friend & Kiang, 2005 for full details). In addition, this methodology clearly

identifies those measurements unlikely to accurately reflect the true ecosystem fluxes because they readily appear as outliers or do not yield a physically realistic solution (cf. Hollinger & Richardson, 2005).

The *Manaus* tropical evergreen rainforest site (Malhi *et al.*, 2002) is used here to illustrate inversion of the flux data and the calibration of the model. The inversion yields a canopy (skin) temperature that is typically raised 1–2 °C above air temperature during the middle of each day, when air temperature is over 30 °C; measured soil temperature increased by 1–2 °C during daylight hours.

Inferred bulk canopy conductance to moisture is shown in Fig. 9a. Canopy conductance peaks around 25 mm [H<sub>2</sub>O] s<sup>-1</sup>, similar to values reported for dry days at this site by Malhi *et al.* (2002). Inferred net canopy  $CO_2$  flux is shown in Fig. 9b. Interestingly, canopy respiration is at least 50% of total respiration due to high canopy temperatures and N content.

Inference of net canopy  $CO_2$  flux allows calculation of the mean canopy surface and internal leaf air space  $CO_2$  ( $C_i$ ) concentrations (Fig. 9c). The gradually falling inferred  $C_i$  values during most days demonstrate increasing restriction of stomatal opening caused by high

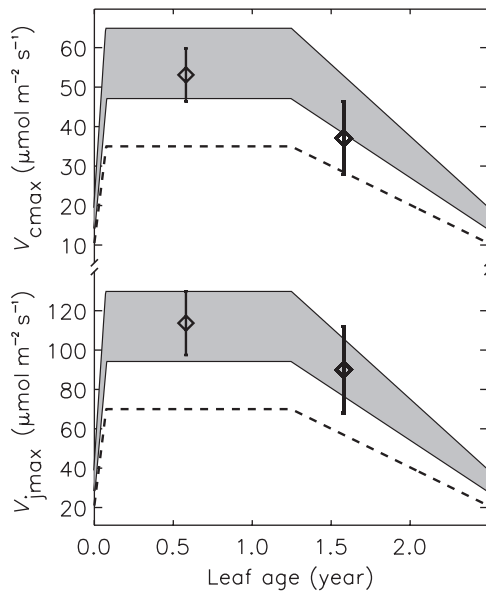


**Fig. 8** Dependency of carboxylation rates  $V_{cmax}$  and  $V_{jmax}$  (at 25 °C) on leaf age in ORCHIDEE for the *a priori* (dashed line) and for the optimized model (grey area). The grey area corresponds to the derived uncertainty on  $K_{vmax}$  (the carboxylation maximum rate multiplier). Independent leaf scale cuvette determinations at Bray for 'young' and 'old' needles (diamonds), with their uncertainties, verify the inverse results.

afternoon air humidity deficits (and perhaps tree-soil hydrological disequilibrium). The mean drop in  $CO_2$  concentration across the canopy leaf surface is about 16%, close to *in situ* measurements (Carswell *et al.*, 2000). Few night-time  $C_i$  values are retrieved by the inversion because the measured  $CO_2$  flux is incompatible with the inferred aerodynamic conductance, suggesting weak coupling between the measured flux and the ecosystem flux (cf. Kruijt *et al.*, 2004).

Canopy quantities were similarly inferred at three further FLUXNET sites: a needle-leaf evergreen plantation (Bray: Berbigier *et al.*, 2001), a mixed cold deciduous forest (Harvard Forest: Wofsy *et al.*, 1993), and a  $C_3$  crop (Ponca: Hanan *et al.*, 2002). Full details are given by Friend & Kiang (2005).

The canopy model was run for each of the four sites using the measured micrometeorological forcing, and inferred canopy temperature, surface  $CO_2$  concentrations, and specific humidity, and was parameterized with site-level measurements of LAI, canopy N, height, and soil moisture. The model was found to perform reasonably well at *Manaus*, but to overpredict bulk canopy conductance and photosynthesis at *Bray*, and underpredict these same quantities at *Harvard Forest* and *Ponca*. The canopy model has two key free parameters, a scaling coefficient between bulk canopy conductance and canopy net photosynthesis at  $C_i \rightarrow \infty$  ( $\alpha$ ),

and the relative proportion of leaf N bound in photosynthetic compounds ( $n_f$ ). These were adjusted for each vegetation type to bring the model into close agreement with the measurements. It was found that once  $n_f$  was calibrated to inferred peak rates of photosynthesis, predicted bulk canopy conductance and  $C_i$  were in reasonable agreement at each site with the same value of  $\alpha$ , and so this was not varied. The resulting fits to inferred canopy conductance,  $CO_2$  flux, and  $C_i$  for *Manaus* are shown in Fig. 9. This vegetation type required  $n_f = 1.1$  (i.e. relative photosynthetic leaf N is 10% higher than the standard values for Rubisco/N and chlorophyll/N given by Kull & Kruijt, 1998). The corresponding calibrated values for the other sites are given in Table 1. Plant types with shorter lived foliage have higher values of  $n_f$ , and thus invest relatively more leaf N in photosynthesis, as would be expected from evolutionary arguments (Reich *et al.*, 1995; Friend & White, 2000).

#### Linking local and global scales

**Global carbon and climate simulations.** The new canopy conductance and  $CO_2$  flux scheme outlined in the last section was incorporated into the latest version of the GISS GCM, ModelE1 (Schmidt *et al.*, 2006), and simulations performed to assess predicted global  $CO_2$  fluxes and climate. Equilibrium climate integrations were performed with the new and old surface schemes using an atmospheric  $CO_2$  concentration of 291 ppmv. Friend & Kiang (2005) give full details of these simulations.

Global seasonal fields of simulated net canopy  $CO_2$  flux are shown in Fig. 10. The total global net canopy  $CO_2$  flux is  $121 Pg [C] yr^{-1}$ , similar to other estimates (Prentice *et al.*, 2001). Absolute seasonal fluxes are greatest in temperate deciduous forests during the northern hemisphere summer, although annual totals are greatest in tropical rainforests.

The new canopy scheme substantially improves simulated climate (Fig. 11). Increased latent heat fluxes from vegetation tend to cool the land surface, which was previously too warm. In addition, precipitation and cloud cover increase in many regions previously too dry and clear. For example, mean JJA cloud cover over the Amazon basin was 10–20% too low using the previous canopy scheme, whereas the new scheme increases cloud cover by 2–6% over the entire basin. Northern winter climate is affected by changes in the global circulation caused by increases in tropical latent heating (Friend & Kiang, 2005).

These large effects result directly from the specification of canopy conductance, both the absolute value and the environmental responses. The new parameterization, calibrated from FLUXNET data (see

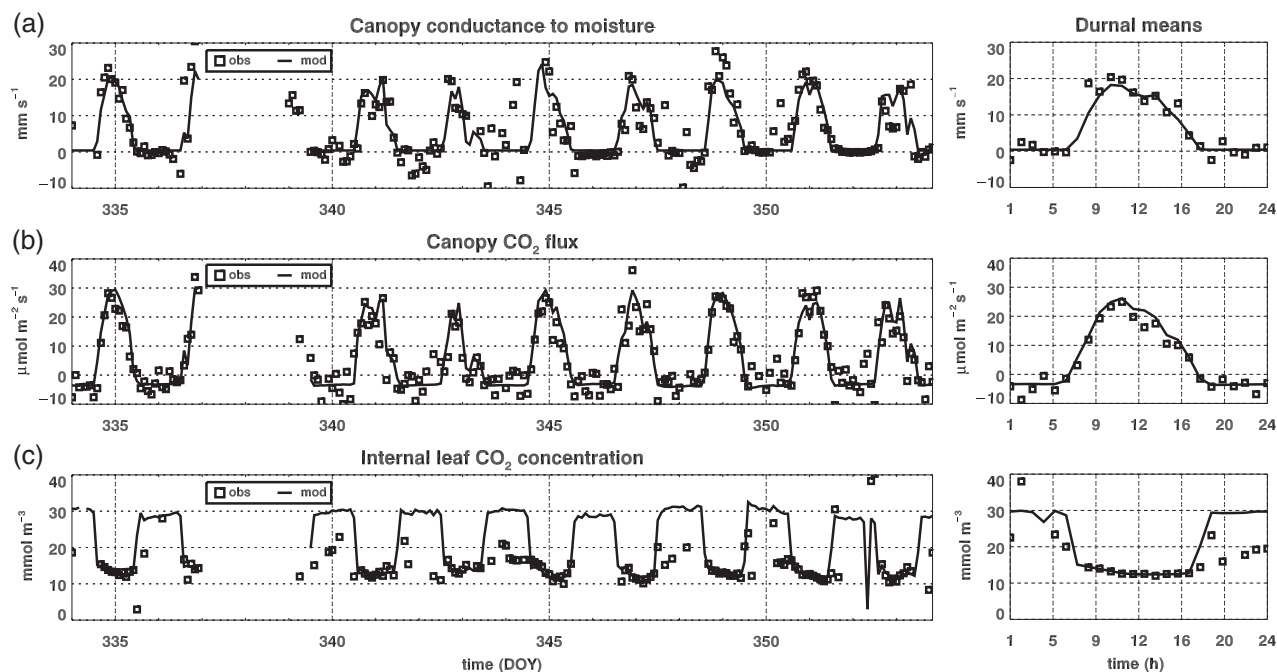


**Fig. 9** Inferred ('obs') and predicted ('mod') variables at the Manaus, Brazil, tropical evergreen forest site (2.59°S, 60.11°W), 11–20 November, 1995. (a) Bulk canopy conductance to moisture; (b) canopy CO<sub>2</sub> flux; (c) mean canopy internal leaf CO<sub>2</sub> concentration. Diurnal means use hourly binning. Model is the Goddard Institute for Space Studies global climate model canopy scheme (Friend & Kiang, 2005).

**Table 1** Calibrated values of the relative proportion of leaf N contained in photosynthetic compounds for each vegetation type used in the GISS GCM

[FLUXNET site	GCM vegetation type							
	Rainforest	Deciduous	Evergreen	Crop	Woodland	Shrub	Grass	Tundra
	<i>Manaus</i>	<i>Harvard Forest</i>	<i>Bray</i>	<i>Ponca</i>				
$n_f$	1.1	1.5	0.9	1.3	1.3	1.3	1.5	1.4

Derived values calculated as follows: 'woodland' = ('rainforest' + 'grass')/2; 'shrub' = 'woodland'; 'grass' = 'deciduous'; 'tundra' = ('shrub' + 'grass')/2.  $\alpha$  is set to 3250 mmol<sup>-1</sup> [CO<sub>2</sub>] at each site (see text).

previous section), substantially increases predicted conductance in most regions, particularly tropical rainforests (Fig. 12). These increases result from the calibration of  $\alpha$  and  $n_f$ , and the more realistic treatment of canopy light and physiological heterogeneity. The addition of the humidity response results in increased conductance in moist regions, although with decreased conductance where the air is very dry; responses reinforced by positive feedbacks with the atmosphere (Friend & Kiang, 2005).

*The role of FLUXNET in validating satellite-derived estimates of surface fluxes.* Operational monitoring of 1 km terrestrial GPP from space has recently become possible following the successful launch and operation of the Moderate Resolution Imaging Spectroradiometer

(MODIS) instrument on board the NASA Terra satellite (Running *et al.*, 2004). FLUXNET is providing a key role in validating this GPP product.

The MODIS GPP algorithm follows the pioneering work of Monteith (1972) and Sellers (1987), who showed, respectively, that vegetation growth is a linear function of absorbed photosynthetically active radiation (APAR), and that APAR could be estimated from remote sensing measurements of the fraction of incident PAR absorbed by the vegetation (FPAR)

$$\text{GPP} = \varepsilon \times \text{APAR} = \varepsilon \times \text{FPAR} \times \text{PAR}, \quad (1)$$

where  $\varepsilon$  is the conversion efficiency of (daily) light energy into vegetation mass. FPAR is calculated from calibrated and atmospherically corrected MODIS measurements of surface reflectances. Integration over

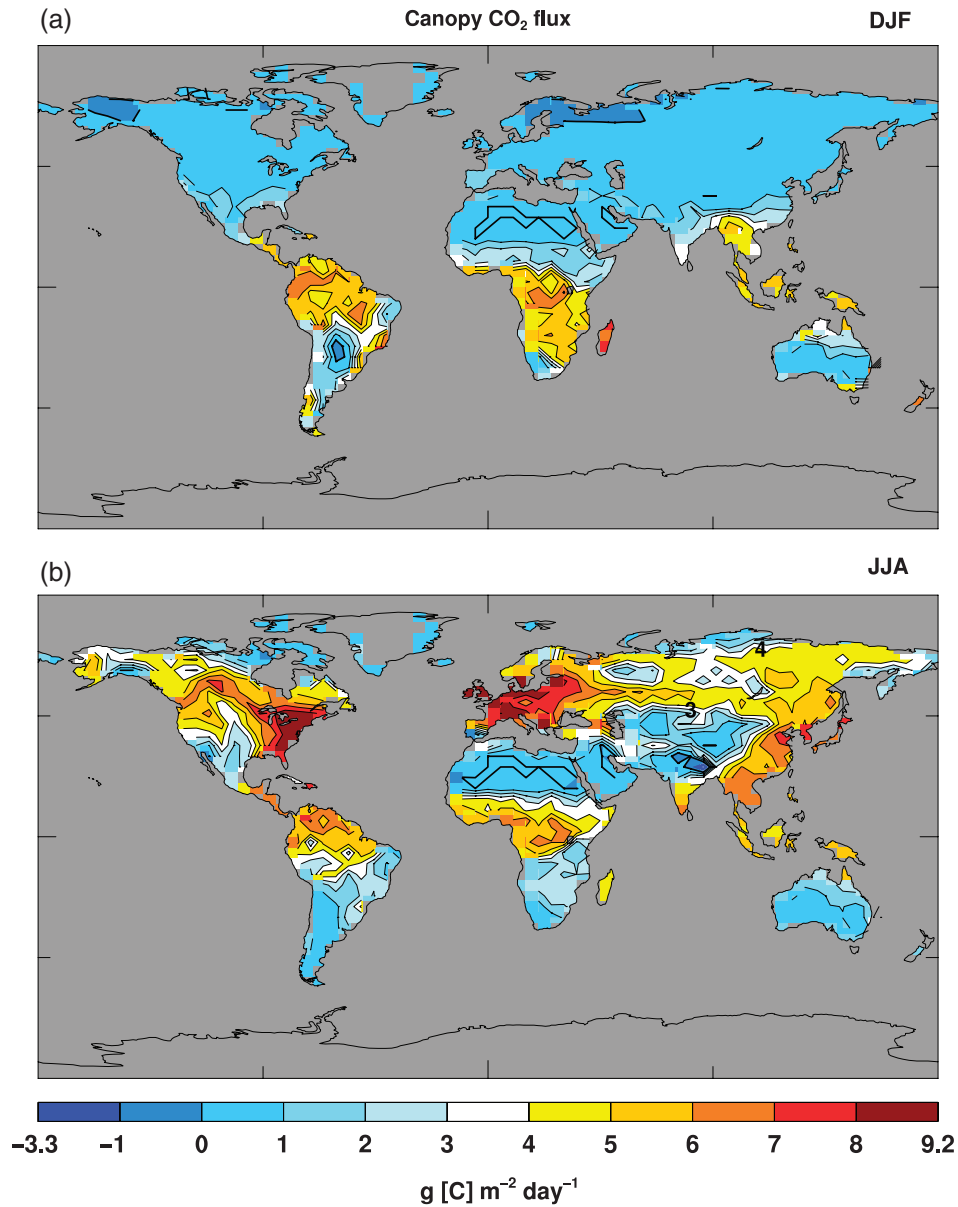


**Fig. 10** Mean December–January–February (DJF) (a) and JJA (b) canopy net CO<sub>2</sub> flux predicted by the Goddard Institute for Space Studies global climate model coupled to the vegetation canopy scheme of Friend & Kiang (2005). Total annual flux is 121 Pg[C]yr<sup>-1</sup>. Values at ends of scale give min and max.

days (*d*) and subtraction of respiration terms gives an estimate of annual net primary production (NPP)

$$NPP = \int_{d=0}^{365} (GPP - R_{lr})dt - R_g - R_m, \quad (2)$$

where  $R_{lr}$  is daily leaf and fine root maintenance respiration,  $R_g$  is annual growth respiration, and  $R_m$  is annual woody tissue maintenance respiration (Running *et al.*, 2000). This algorithm is known as the ‘PEM’. Constraints on GPP due to low temperatures

or high vapour pressure deficits (VPDs) reduce  $\epsilon$ . Vegetation- (i.e. evergreen needle-leaved forest, deciduous broad-leaved forest, shrubland, savanna, grassland, and cropland) specific maximum values for  $\epsilon$ , and the temperature and VPD limits are computed using the detailed ecosystem model BIOME-BGC (White *et al.*, 2000). Meteorological forcing (i.e. mean daily temperature, daily minimum temperature, air vapour pressure, and incident shortwave radiation) is provided by the NASA Data Assimilation Office (DAO) from interpolation of *in situ*

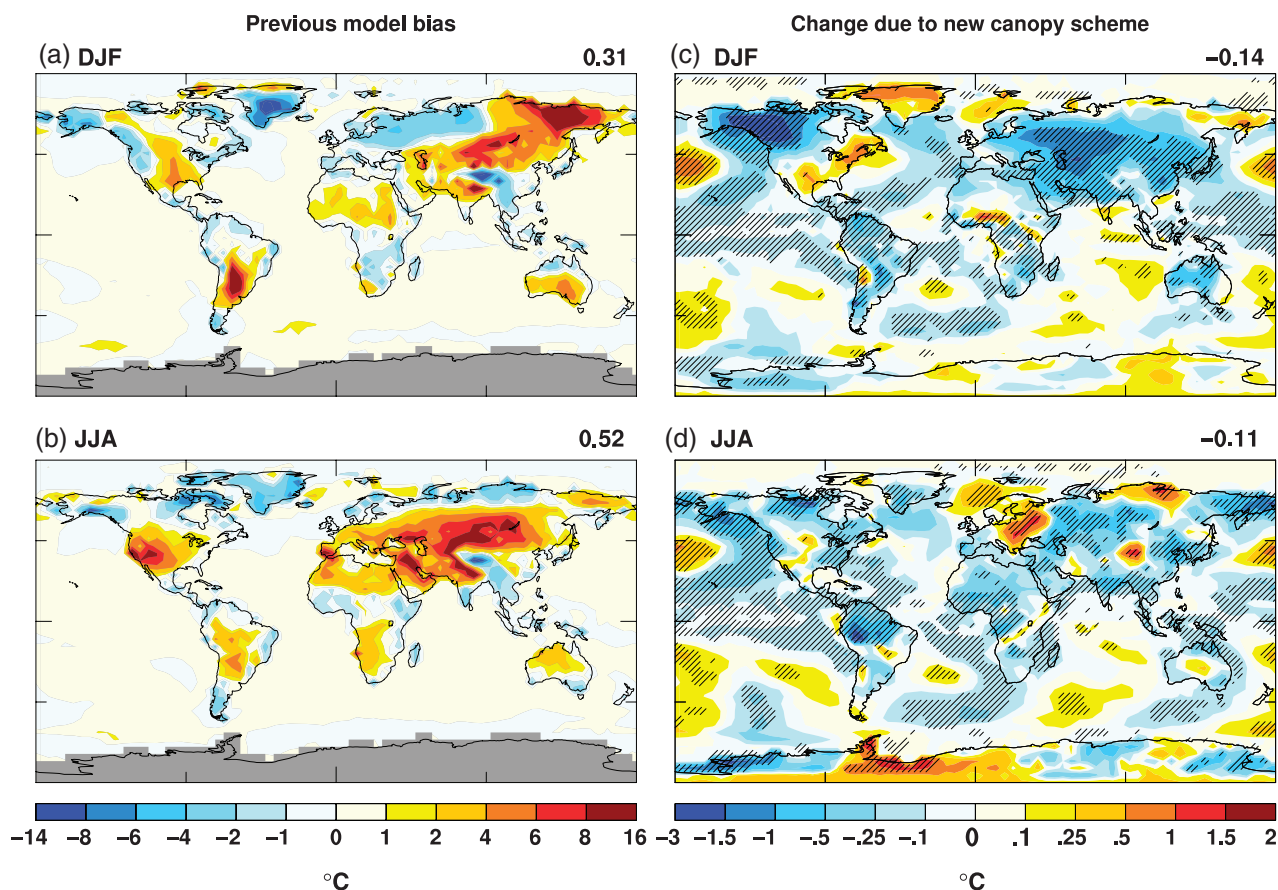


**Fig. 11** Seasonal mean surface temperature bias of Goddard Institute for Space Studies global climate model using previous canopy scheme (December–January–February (DJF), a; JJA, b), and change in seasonal surface temperature due to new canopy scheme of Friend & Kiang (2005) (DJF, c; JJA, d). Observations are merged land air temperatures (New *et al.*, 1999) and sea surface temperatures (Rayner *et al.*, 2003). Global means at upper-right corners. Absolute ranges:  $-13.6^{\circ}\text{C}$  to  $+16.1^{\circ}\text{C}$  (a);  $-12.5^{\circ}\text{C}$  to  $+12.9^{\circ}\text{C}$  (b);  $-2.8^{\circ}\text{C}$  to  $+1.2^{\circ}\text{C}$  (c); and  $-2.2^{\circ}\text{C}$  to  $+1.8^{\circ}\text{C}$  (d). Hatched areas significant at the 95% confidence level for a paired *t*-test. Figure redrawn from Friend & Kiang (2005).

measurements. GPP is calculated for each 8-day period at 1 km global resolution.

FLUXNET data are the primary source of information for validating this GPP product. GPP is compared directly with measurements made by all FLUXNET eddy covariance towers using a  $7 \times 7 \text{ km}^2$  sample of the MODIS product located around each tower. The seasonality of daily measured GPP is well characterized across different climates (Fig. 13). However, springtime GPP is underestimated, whereas midsummer GPP is overestimated, compared with the measurements. The overestimate results from insufficient drought constraints in the GPP algorithm. However, much of this midsummer bias occurs because the DAO meteorology is not local to the flux tower, demonstrated by rerunning the GPP algorithm using *in situ* meteorology (Fig. 13). DAO data are rather coarse resolution ( $1^{\circ} \times 1.25^{\circ}$ ), and so cannot capture tower-scale conditions adequately, particularly local VPD.

*Global variability in NPP.* The MODIS NPP algorithm outlined above was used to investigate variability in global NPP for 1982–1999 using AVHRR satellite data and NCEP daily reanalysis meteorological fields (Nemani *et al.*, 2003). A significant finding is that global NPP increased by 6.17% over this 18 year period, with the Amazon basin contributing 42% of this increase (Fig. 14). Interannual variability was  $\pm 1.5\%$  of total NPP. Increased NPP results partly from reductions in temperature, moisture, and, particularly, radiation constraints on plant growth. The large Amazon basin response appears to be due to falling cloud cover causing increased radiation, whereas the large increase in NPP for north-western North America results from higher spring temperatures and longer growing seasons. Additional simulations using climatological *FPAR* showed that climate changes contributed 40% of the NPP increase and changes in leaf area contributed 60%.

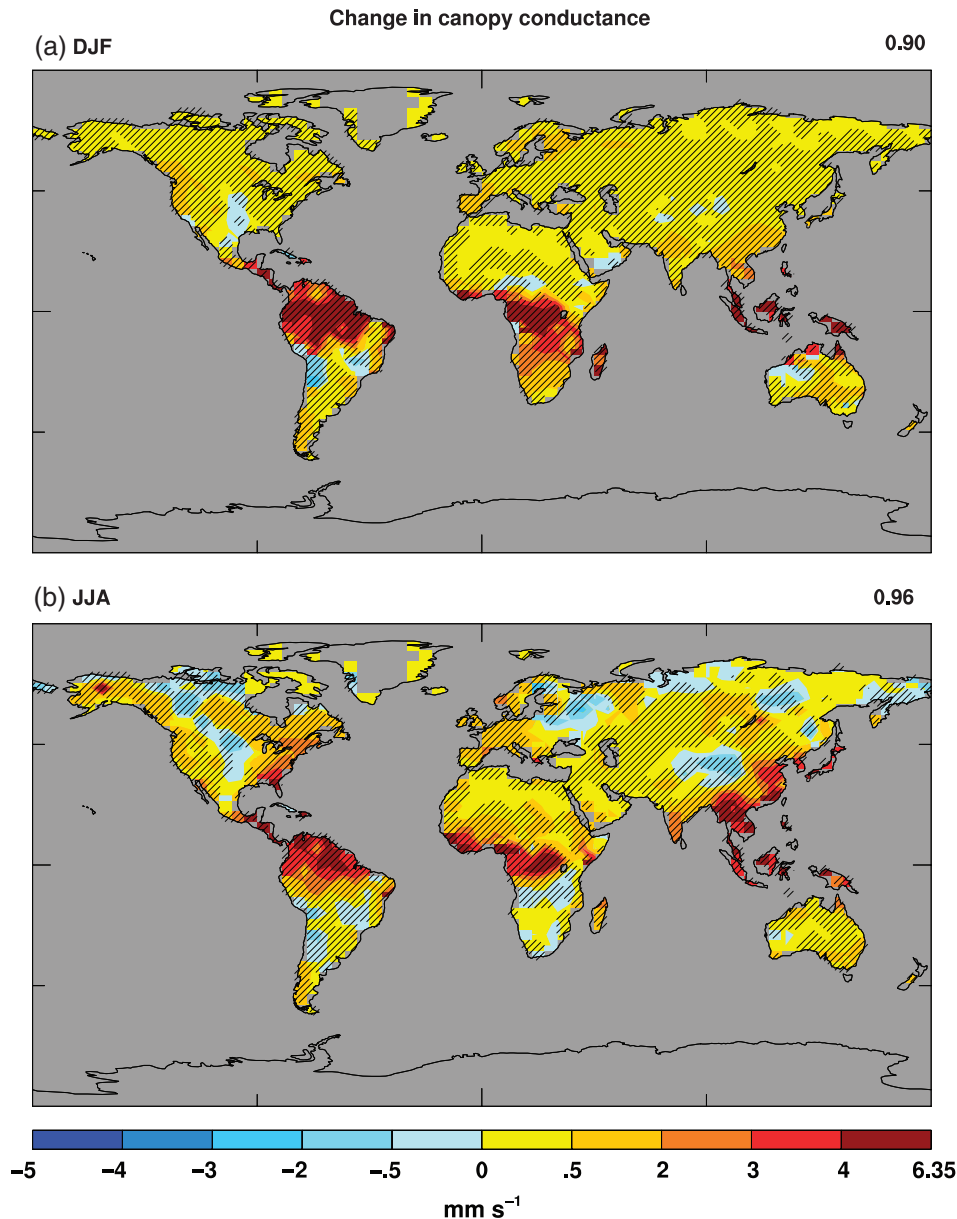


**Fig. 12** Change in mean seasonal canopy stomatal conductance to moisture due to replacement of Goddard Institute for Space Studies global climate model canopy scheme with that of Friend & Kiang (2005). December–January–February (DJF) (a) absolute range:  $-3.0$  to  $+6.4$   $\text{mm s}^{-1}$ ; JJA (b) absolute range:  $-2.7$  to  $+6.3$   $\text{mm s}^{-1}$ . Global non-Antarctica land means at upper-right corners. Hatched areas are significant at the 95% confidence level for a paired *t*-test. Figure redrawn from Friend & Kiang (2005).

These findings are examined further in the *Discussion* below.

#### *Towards linking FLUXNET and atmospheric flask CO<sub>2</sub> data*

*Inversion of atmospheric CO<sub>2</sub> measurements.* The atmosphere integrates all surface fluxes of CO<sub>2</sub>, making atmospheric measurements of spatial and

temporal variations in CO<sub>2</sub> concentrations a powerful tool for understanding the global carbon cycle. An increasingly large global network of sites has been measuring atmospheric CO<sub>2</sub> since the 1950s, but quantitative interpretation of these measurements in terms of regionally resolved surface fluxes requires application of an atmospheric transport model in inverse mode. In the context of interannual variations in CO<sub>2</sub> fluxes, the time-dependent Bayesian inversion

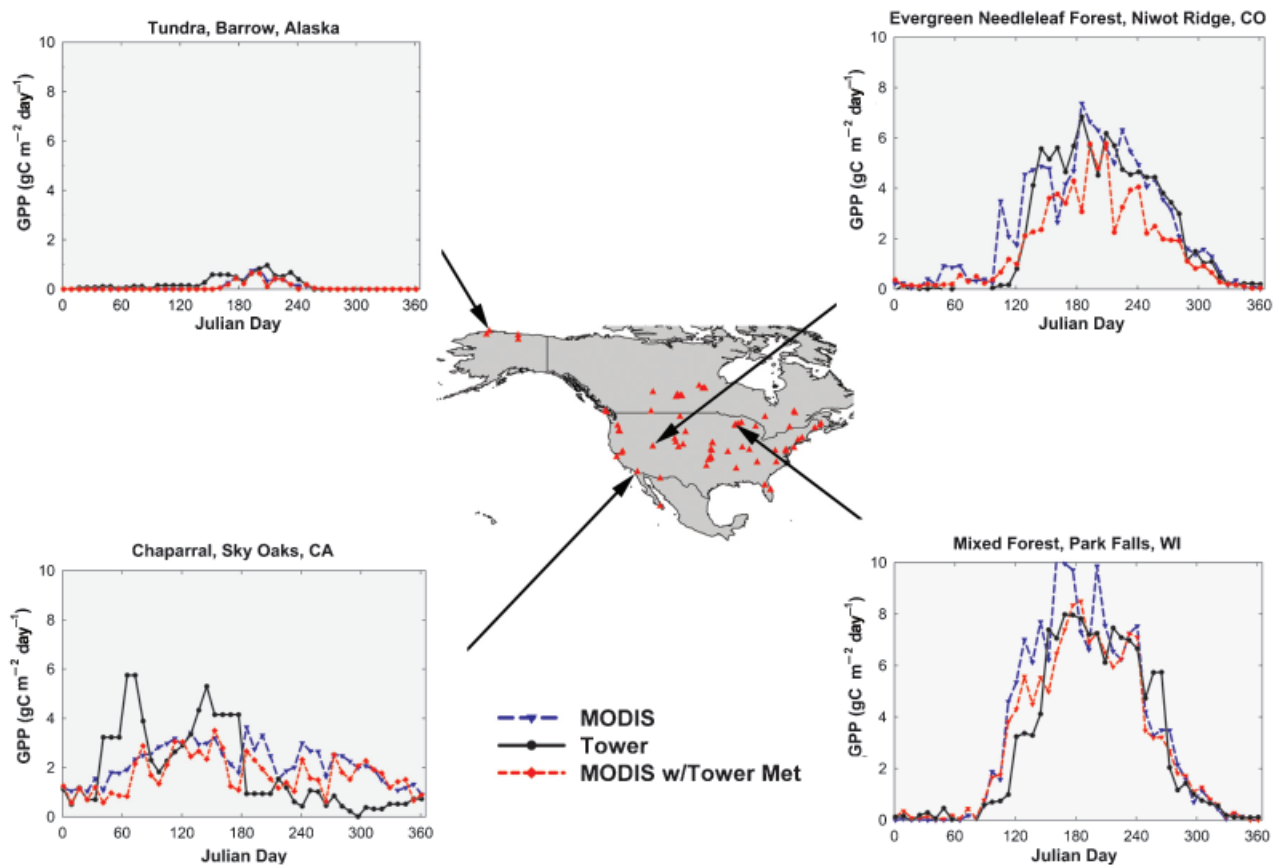


Fig. 13 Intercomparison of MODIS 8 day gross primary production (GPP) product with FLUXNET GPP measurements in 2001. Substituting *in situ* meteorological data for the lower resolution Data Assimilation Office operational data allows separation of model bias errors. Figure redrawn from Running *et al.* (2004).

technique was first applied by Rayner *et al.* (1999). Subsequent studies updated this methodology, including detailed uncertainty analysis, to further extend our understanding on surface controls of CO<sub>2</sub> fluxes (e.g. Bousquet *et al.*, 2000; Rödenbeck *et al.*, 2003; Peylin *et al.*, 2005).

The increasing number of active atmospheric measurement sites makes inverse estimates of surface fluxes increasingly robust. Before the 1990s, the number of sites was rather low, but more than 100 sites are now available. In the study by Rödenbeck *et al.* (2003), reviewed here as an example, flask CO<sub>2</sub> data were obtained from the NOAA/CMDL sampling network (an update of Conway *et al.*, 1994). Up to 35 sites were selected that covered different multiyear periods without any large gaps. Atmospheric transport was calculated using the global atmospheric transport model TM3 (Heimann, 1996), driven by interannual meteorological fields derived from the NCEP reanalysis (Kalney *et al.*, 1996).

Because the available spatial coverage of concentration data is low relative to the global inverse problem, *a priori* information is required to establish the most likely pattern of surface fluxes. In Rödenbeck *et al.* (2003), *a priori* information consisted of statistics of anthropogenic emissions from fossil fuel burning and cement manufacturing (Olivier & Berdowski, 2001), climatological NEE of the terrestrial biosphere (mean seasonal cycle over 1980–1992 as estimated by LPJ, Sitch *et al.*, 2000), and ocean-atmosphere C exchange (Takashi *et al.*, 1999; Gloor *et al.*, 2003). The adjustments of fluxes from these *a priori* values by the inversion are weighted according to fixed spatio-temporal distributions. For terrestrial NEE, this weighting was chosen proportional to mean NPP. Therefore, the inversion preferentially adjusts fluxes in locations with high vegetation activity, such as tropical rainforest. Spatial and temporal correlations of the flux adjustments are also specified, determining their spatio-temporal coherence scales. Correlation scales for NEE were set to

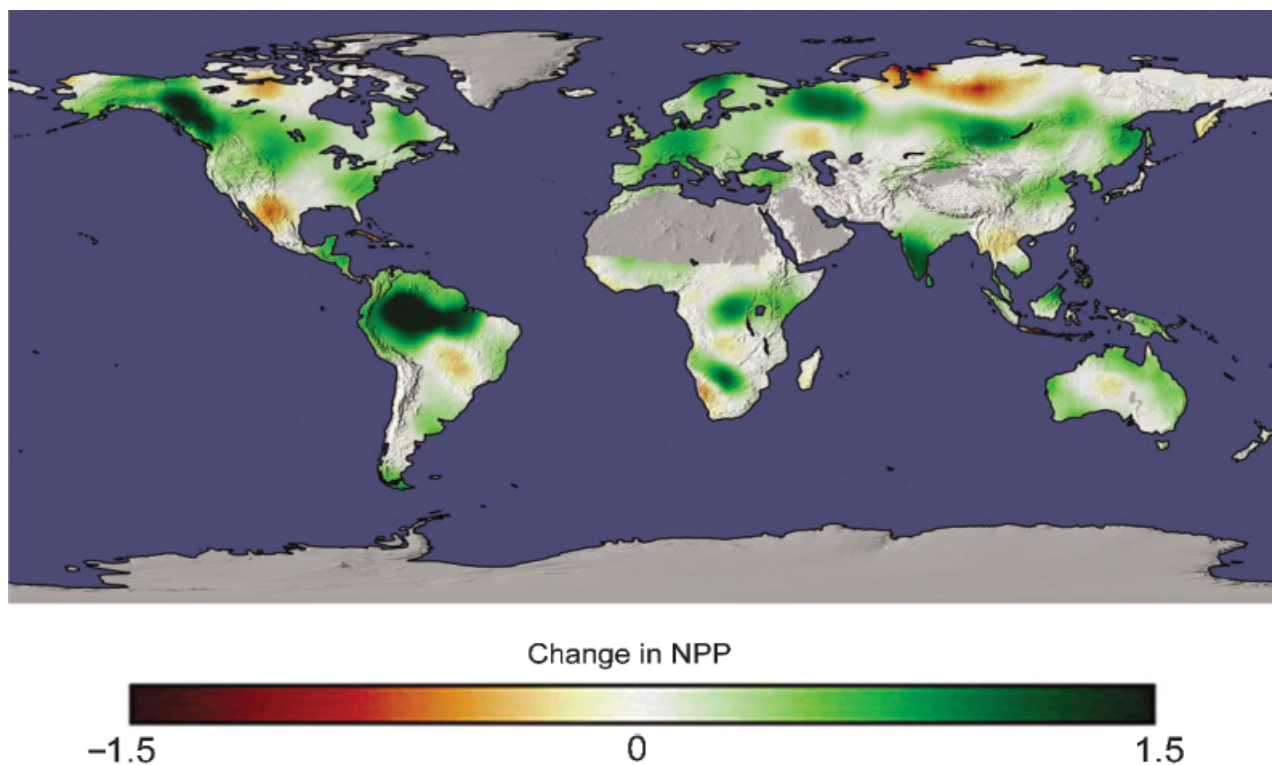


Fig. 14 Trends in net primary production (NPP) 1982–1999 computed using the production efficiency model, driven by AVHRR NDVI (percentage change per year). Figure redrawn from Nemani *et al.* (2003).

about 1200 km, corresponding to scales of synoptic weather phenomena.

*Inversion-estimated surface flux anomalies.* The interpolated atmospheric CO<sub>2</sub> data and estimated surface CO<sub>2</sub> flux anomalies for 1982–2000 are shown over latitude and time in Fig. 15, together with the Oceanic Niño Index (ONI). El Niño events display high ONI temperatures, and are clearly one of the major drivers of both the temporal and spatial variability in atmospheric CO<sub>2</sub>. (Fig. 15a). A significant period of negative surface anomalies following the Mount Pinatubo eruption is also evident (Fig. 15b). The inversion localizes flux anomalies on a finer resolution. The tropical land surface is estimated to be the main driver of the atmospheric anomalies (Fig. 15c),

particularly in response to El Niño and La Niño periods, except for the 2 years after the Pinatubo eruption.

Much of the El Niño/Southern Oscillation (ENSO) variability effect is found in Tropical and South America. For example, Fig. 16 shows the surface distribution for the flux anomaly during the strong 1997/1998 El Niño event. These anomalies are closely correlated with large changes in tropical precipitation. Large biomass burning events seem to be an important mechanism for C emissions, as indicated by satellite estimates (cf. Rödenbeck *et al.*, 2003).

There is good agreement between estimates of regional CO<sub>2</sub> flux variability from atmospheric inversions and two process-based land models (LPJ and SLAVE) (Peylin *et al.*, 2005). The largest uncertainty

Fig. 15 (a) Measured atmospheric CO<sub>2</sub> growth rate anomalies (longitudinal annual means linearly interpolated between measurement sites); (b) surface CO<sub>2</sub> flux anomalies as estimated by inversion; (c) as (b) except land fluxes only; (d) as (b) except ocean fluxes only. Colour spectra show anomaly amplitude; white spaces separate periods of increasing numbers of measurement sites. Also shown (e) is the Oceanic Niño Index (ONI; NOAA: [http://www.cpc.ncep.noaa.gov/products/analysis\\_monitoring/ensostuff/ensoyears.shtml](http://www.cpc.ncep.noaa.gov/products/analysis_monitoring/ensostuff/ensoyears.shtml)), and the time of the Mt Pinatubo volcanic eruption (purple arrow). Vertical brown lines show timing of peak Oceanic Niño Index values, indicating strong El Niño conditions. Figure redrawn from Rödenbeck *et al.* (2003).



among these models is in the response of the decomposition of organic material to both precipitation and temperature (Peylin *et al.*, 2005).

*Potential uses of FLUXNET data in inversions.* As the *a priori* constraints have considerable impact on estimated fluxes, reliability of inversion results can potentially be improved by using additional data sources. Clearly, FLUXNET data represent such a source of information. Unfortunately, a direct incorporation of eddy flux measurements into the atmospheric inversion calculation is difficult, because the spatial scales seen from the atmospheric concentration gradients are much larger than the footprint of measured fluxes. However, a possible way to close the gap in scales between these data streams is to use carbon cycle models. Validation of process models using FLUXNET data (as well as calibration of remote-sensing driven diagnostic models), as outlined in the previous sections, and then use of these models to simulate regional and global fluxes, represents a step in this direction. In a more elaborate framework, optimization of model parameters can be based both on FLUXNET data and on atmospheric data; a prototype of such a 'data assimilation system' has recently been published by Rayner *et al.* (2005).

As a method of intermediate complexity, flux data could also provide statistical information to be used as *a priori* constraints in the inversion. For example, multiyear flux time series from sufficient numbers of different locations and biome types could give spatial

patterns of amplitudes of seasonal or interannual variability, replacing the crude vegetation proxies mentioned above. Furthermore, correlation analysis of flux time series, both autocorrelation in time and cross-correlation between sites, could yield valuable information on the structure of spatio-temporal coherence of fluxes, replacing the *ad hoc* specification of correlation lengths generally used so far. Similarly, spectral or wavelet analysis of measured fluxes can give *a priori* information in the time dimension.

## Discussion

Eddy covariance measurements of ecosystem-atmosphere CO<sub>2</sub>, energy, and moisture fluxes are indispensable for the attribution of mechanisms to the observed temporal and spatial variability in the global carbon cycle. The various applications of FLUXNET eddy covariance data reviewed here demonstrate how these data have been used to evaluate and calibrate DGVMs, have led to substantial improvements in simulated climate in a GCM, show promising utility for model parameter estimation, underpin global operational vegetation productivity products, and could be used in future global CO<sub>2</sub> atmospheric inversion studies.

What do these global studies tell us about the contemporary C cycle? Certainly the 6.2% increase in global NPP over the period 1982–1999 simulated by the PEM is an important finding that demands careful analysis. Additional simulations, with constant vegetation or constant climate, showed that the majority of the increase in NPP could be attributed to vegetation changes

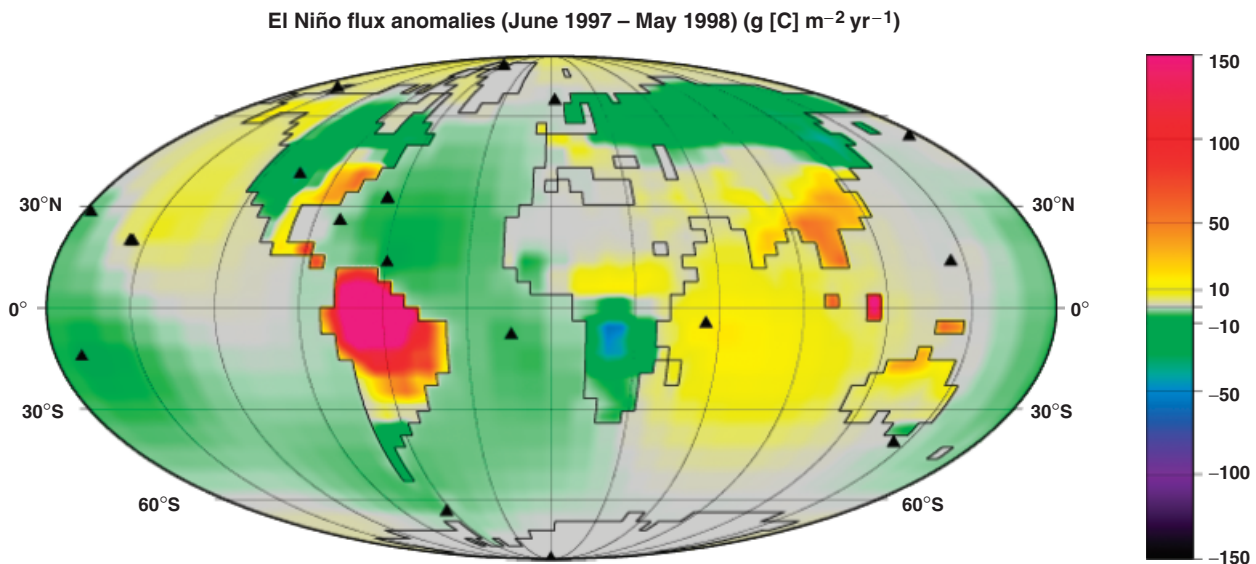


**Fig. 16** Spatial pattern of inversion-estimated mean surface CO<sub>2</sub> flux anomalies during the 1997/1998 El Niño period relative to the 1990–1999 mean, estimated with 19 atmospheric measurement sites (solid triangles). Figure redrawn from Rödenbeck *et al.* (2003).

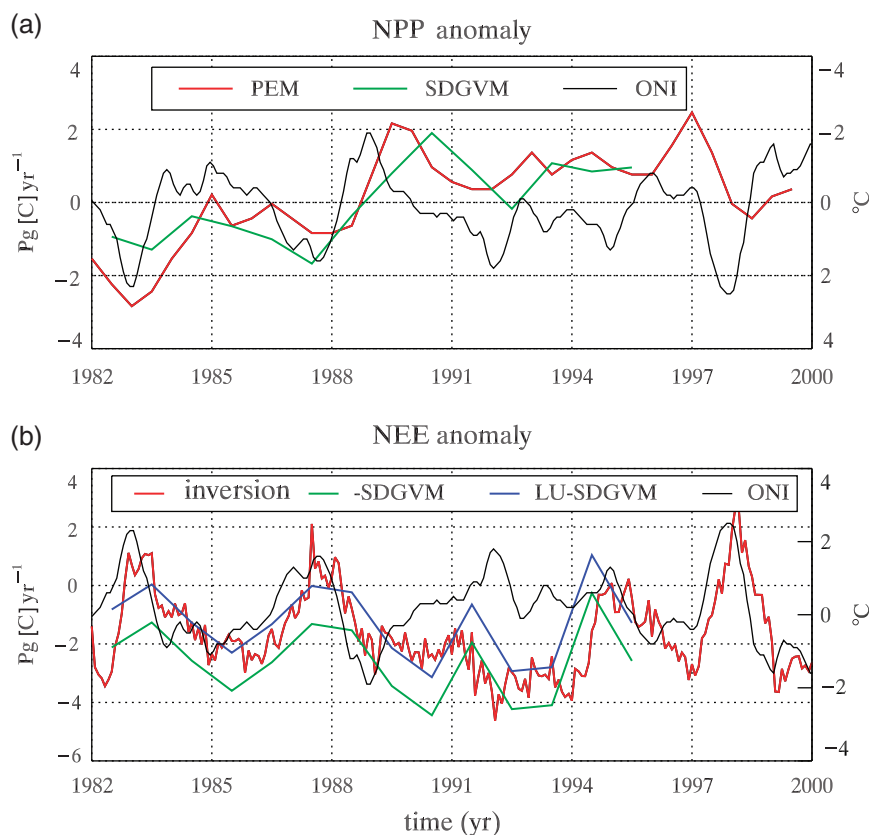


**Fig. 17** (a) Global net primary production (NPP) anomaly estimated by the production efficiency model (PEM) relative to its 1982–1995 mean (red line); annual NPP anomaly predicted by the SDGVM relative to its 1982–1995 mean (green line); Oceanic Niño Index (black line, inverted scale). (b) Global running yearly sum of monthly estimates of land net ecosystem exchange of CO<sub>2</sub> (NEE) estimated by inversion of atmospheric CO<sub>2</sub> measurements (red line, nonfossil fuel fluxes; number of sites increasing from 11 to 35 with time, see Rödenbeck *et al.*, 2003), mean annual NEE predicted by the SDGVM (green line), same plus calibrated land use flux of 1.3 Pg [C] yr<sup>-1</sup> (blue line). Oceanic Niño Index also shown (see Fig. 15), with direct scale (black line).

resulting in increased light absorption (Nemani *et al.*, 2003). Climate alone accounted for 39% of the increase to 1996, but was not a significant factor over the entire 1982–1999 study period due to the 1997–1998 El Niño. Changes in vegetation structure could have arisen from a variety of processes, including growth stimulation by increasing CO<sub>2</sub> and/or N deposition, climate-vegetation feedbacks, and land use.

The global SDGVM simulation also predicts increasing NPP over this period, and therefore allows further investigation into the causes of this change. Despite different absolute NPP (PEM: 54.5 Pg [C] yr<sup>-1</sup>; SDGVM: 74.3 Pg [C] yr<sup>-1</sup>), both models predict very similar NPP variability over the period 1982–1995 (the years when both approaches were applied), with interannual variability largely driven by ENSO (Fig. 17a). The major reason for the increasing NPP in the SDGVM is the effect of CO<sub>2</sub> on photosynthesis and water use efficiency, with lesser contributions from increasing temperature and N deposition (Woodward & Lomas, 2004). These effects would be expected to have significant

impacts on leaf area, and are therefore observed from space and likely drive the increase in NPP in the PEM (the PEM algorithm does not include CO<sub>2</sub> concentration directly). Therefore, CO<sub>2</sub> fertilization of photosynthesis appears to be a key process in the contemporary response of the terrestrial biosphere to global change, but has been a controversial aspect of the global carbon cycle. This finding is strongly supported by additional GISS GCM simulations, where doubled CO<sub>2</sub> substantially increased global photosynthesis (+47%), whereas climate change alone caused reduced CO<sub>2</sub> uptake (−9%).

The SDGVM also predicts total ecosystem CO<sub>2</sub> exchange with the atmosphere, allowing comparison with the inversion model results, and extension of the PEM result to the net terrestrial CO<sub>2</sub> flux. The mean net terrestrial flux for 1982–1995 is calculated by the SDGVM to be −2.6 Pg [C] yr<sup>-1</sup>, whereas the inversion of atmospheric measurements gives a net flux of −1.2 Pg [C] yr<sup>-1</sup>, although with considerable uncertainty. The SDGVM does not include the C flux from

land use, which is highly uncertain but thought to have been in the range  $0.6\text{--}2.5\text{Pg [C] yr}^{-1}$  for this period (see DeFries *et al.*, 2002, for evidence that the actual value is towards the low end of this range). Figure 17b compares the predicted net flux from the SDGVM before and after calibration with a constant land use flux correction of  $1.3\text{Pg [C] yr}^{-1}$ , together with the inversion-based flux and the ENSO index. The match is fairly close, with ENSO the main driver of interannual variability. A notable exception is the El Niño event that peaks in January 1992, but is not associated with an observed reduction in terrestrial C uptake, although such an effect is somewhat predicted by the model. The eruption of Mt Pinatubo in the Philippines in June 1991 has been invoked to explain the anomalous terrestrial C uptake inferred by the atmospheric measurements (Gu *et al.*, 2003), but the mechanism remains controversial (Robock, 2005). The SDGVM somewhat underpredicts the magnitude of the observed net C uptake following the eruption, suggesting that additional processes such as the greater efficiency of diffuse light for canopy photosynthesis may need to be invoked (Gu *et al.*, 2003).

The PEM predicts that the Amazon basin largely drives variability in global NPP. The atmospheric inversion also points to this region as the main source of ENSO-driven global carbon cycle dynamics, although this is at least partly a result of the *a priori* NEE distribution pattern simulated by the LPJ model. The inversion estimates a net flux of  $-0.6 \pm 0.3\text{Pg [C] yr}^{-1}$  in the South American Tropical region for the 1990s, implying a natural ecosystem flux of  $-0.8$  to  $-1.3\text{Pg [C] yr}^{-1}$  after allowing for land use change (Rödenbeck *et al.*, 2003). Field biometry measurements point to a somewhat smaller natural Amazonian flux of  $-0.4$  to  $-0.6\text{Pg [C] yr}^{-1}$  (Phillips *et al.*, 1998), whereas flux tower measurements suggest a much larger sink (Miller *et al.*, 2004). The inversion-based sink for this region has a maximum of about  $150\text{g [C] m}^{-2}\text{yr}^{-1}$ , or  $1.5\text{Mg [C] ha}^{-1}\text{yr}^{-1}$ , whereas flux towers have measured uptake as high as  $6\text{Mg [C] ha}^{-1}\text{yr}^{-1}$  (Malhi *et al.*, 1998). There is, however, substantial uncertainty with respect to night-time fluxes for Amazon forests (and presumably all dense forests), making scaling up fluxes in time very problematical (Kruijt *et al.*, 2004). Clearly, reducing the gap between *in situ* tropical rainforest and global atmospheric measurements must be a priority for future terrestrial carbon cycle research.

An important point regarding the generality of global carbon cycle models arises from the mismatch between modelled and observed NEE at FLUXNET sites where night-time fluxes are thought to pose no major problems. If the general model 'error' ('bias' is probably a better term) of net C uptake arises because of the effects of management, then the model should still be applic-

able globally where the majority of forests are unmanaged, and management can be built into the global model where it is important (e.g. for Europe such as in Zaehle *et al.*, 2006). If, however, the mismatch results from some fundamental model inadequacy, then model utility is severely compromised. This issue merits careful future research, underpinned by improved knowledge concerning the management history of FLUXNET sites.

Finally, a number of recommendations arise from the studies outlined here. Meaningful comparisons of short-term model behaviour with flux measurements demand accurate estimates of a number of site parameters such as canopy N, LAI, and soil moisture, but these are often difficult or impossible to find, therefore reducing the value of such comparisons and of eddy covariance data. Longer-term comparisons require biomass and soil C data or estimates, enabling separation of fast and slow C processes. As is clear from this paper, information on site history is important in order to make a full evaluation of a model's performance. It is recognized that this is not always available, but even anecdotal evidence of past land use or disturbance would be of significant help. Other recommendations include an increase in the number of measurement towers at locations as little disturbed by human management as possible, as well as in important tropical ecosystems such as savannas and wetlands, and in very high northern tundra and wetlands. Finally, there is currently a lack of representation of the full life cycle of ecosystems, including burnt, diseased, overthrown, or cut sites, as well as ecosystems approaching the end of their natural life cycle.

The greatest value for current FLUXNET data in developing models is in evaluating their representation of processes, rather than providing an unbiased estimate of net C exchange. Therefore, gap-filled data are of limited use for modellers, and if provided need to be carefully separated from primary *in situ* data so as to avoid model-model comparisons. Indeed, carefully designed campaign-type studies of limited temporal coverage, but comparing a range of ecosystems in a given region, may usefully complement long-term observation sites, addressing some of the issues raised in the previous paragraph with a defensible logistical effort. Finally, the calculation and provision of uncertainty estimates should be a part of all *in situ* measurement campaigns if their data are to be used to rigorously validate and parameterize global carbon models.

### Acknowledgements

We wish to thank Dennis Baldocchi and the FLUXNET office at Oak Ridge National Laboratory for creating an indispensable

tool for global environmental research, and the many investigators whose data have contributed to the work discussed here. We thank Reto Reudy for his patient assistance with GISS GCM simulations and all the GISS model development team. Yadvinder Malhi, Paul Berbigier, Denis Loustau, and George Burba provided flux data, and Joe Berry provided leaf N data for *Ponca*. ADF and NYK were partly sponsored by DOE grant DE-FG02-02ER63444, of the Office of Science, Scientific Discovery through Advanced Computing, Climate Change Prediction Program. ADF and NYK thank Jack Kaye, Don Anderson, and Tsengdar Lee of NASA Headquarters for support of their research. ADF also acknowledges support by the CNRS (France), the CNRS INSU ECCO Programme, and the European Commission's Sixth Framework Programme Marie Curie Research Training Networks Action. FIW and MRL were supported by the NERC (UK).

## References

- Aubinet M, Grelle A, Ibrom A *et al.* (2000) Estimates of the annual net carbon and water exchange of European forests: the EUROFLUX methodology. *Advances in Ecological Research*, **30**, 113–175.
- Baldocchi D, Falge E, Gu L *et al.* (2001) FLUXNET: a new tool to study the temporal and spatial variability of ecosystem-scale carbon dioxide, water vapor, and energy flux densities. *Bulletin of the American Meteorological Society*, **82**, 2415–2434.
- Berbigier F, Bonnefond J-M, Mellmann P (2001) CO<sub>2</sub> and water vapour fluxes for 2 years above Euroflux forest site. *Agricultural and Forest Meteorology*, **108**, 183–197.
- Bousquet P, Peylin P, Ciais P *et al.* (2000) Regional changes in carbon dioxide fluxes of land and oceans since 1980. *Science*, **290**, 1342–1346.
- Carswell FE, Meir P, Wandelli EV *et al.* (2000) Photosynthetic capacity in a central Amazonian rain forest. *Tree Physiology*, **20**, 179–186.
- Conway TJ, Tans PP, Waterman LS *et al.* (1994) Evidence for interannual variability of the carbon cycle from the National Oceanic and Atmospheric Administration/Climate Monitoring and Diagnostics Laboratory Global Air Sampling Network. *Journal of Geophysical Research*, **99**, 22831–22855.
- Cramer W, Bondeau A, Woodward FI *et al.* (2001) Global response of terrestrial ecosystem structure and function to CO<sub>2</sub> and climate change: results from six dynamic global vegetation models. *Global Change Biology*, **7**, 357–373.
- DeFries RS, Houghton RA, Hansen MC *et al.* (2002) Carbon emissions from tropical deforestation and regrowth based on satellite observations for the 1980s and 1990s. *Proceedings of the National Academy of Sciences*, **99**, 14256–14261, doi: 10.1073/pnas.182560099.
- Dore S, Hymus GJ, Johnson DP *et al.* (2003) Cross validation of open-top chamber and eddy covariance measurements of ecosystem CO<sub>2</sub> exchange in a Florida scrub-oak ecosystem. *Global Change Biology*, **9**, 84–95.
- Falge E, Baldocchi D, Olson R *et al.* (2001) Gap filling strategies for defensible annual sums of net ecosystem exchange. *Agricultural and Forest Meteorology*, **107**, 43–69.
- Francey RJ, Tans PP, Allison CE *et al.* (1995) Changes in oceanic and terrestrial carbon uptake since 1982. *Nature*, **373**, 326–330.
- Franks SW, Bevan KJ (1997) Bayesian estimation of uncertainty in land surface-atmosphere flux predictions. *Journal of Geophysical Research*, **102**, 23991–23999.
- Friedlingstein P, Dufresne J-L, Cox PM *et al.* (2003) How positive is the feedback between climate change and the carbon cycle? *Tellus B*, **55**, 692–700.
- Friend AD, Kiang NY (2005) Land surface model development for the GISS GCM: effects of improved canopy physiology on simulation climate. *Journal of Climate*, **18**, 2883–2902.
- Friend AD, White A (2000) Evaluation and analysis of a dynamic terrestrial ecosystem model under preindustrial conditions at the global scale. *Global Biogeochemical Cycles*, **14**, 1173–1190.
- Gloor M, Gruber N, Sarmiento J *et al.* (2003) A first estimate of present and preindustrial air-sea CO<sub>2</sub> flux patterns based on ocean interior carbon measurements and models. *Geophysical Research Letters*, **30**, 10-1–10-4, doi: 10.1029/2002GL015594.
- Goodale CL, Apps MJ, Birdsey RA *et al.* (2002) Forest carbon sinks in the northern hemisphere. *Ecological Applications*, **12**, 891–899.
- Gu L, Baldocchi DD, Wofsy SC *et al.* (2003) Response of a deciduous forest to the Mount Pinatubo eruption: enhanced photosynthesis. *Science*, **299**, 2035–2038.
- Gupta HV, Bastidas LA, Sorooshian S *et al.* (1999) Parameter estimation of a land surface scheme using multicriteria methods. *Journal of Geophysical Research*, **104**, 19491–19503.
- Hanan NP, Burba G, Verma SB *et al.* (2002) Inversion of net ecosystem CO<sub>2</sub> flux measurements for estimation of canopy PAR absorption. *Global Change Biology*, **8**, 563–574.
- Heimann M (1996) *The global atmospheric transport model TM2*. Technical Report 10, Max-Planck-Institut für Meteorologie, Hamburg, Germany.
- Hollinger DY, Richardson AD (2005) Uncertainty in eddy covariance measurements and its application to physiological models. *Tree Physiology*, **25**, 873–885.
- Houghton RA (2003) Why are estimates of the terrestrial carbon balance so different? *Global Change Biology*, **9**, 500–509.
- Ishida A, Uemura A, Koike N *et al.* (1999) Interactive effects of leaf age and self-shading on leaf structure, photosynthetic capacity and chlorophyll fluorescence in the rain forest tree, *Dryobalanops aromatica*. *Tree Physiology*, **19**, 741–747.
- Janssens IA, Freibauer A, Ciais P *et al.* (2003) Europe's terrestrial biosphere absorbs 7 to 12% of European anthropogenic CO<sub>2</sub> emissions. *Science*, **300**, 1538–1542.
- Jones CD, Cox P, Huntingford C (2003) Uncertainty in climate – carbon-cycle projections associated with the sensitivity of soil respiration to temperature. *Tellus B*, **55**, 642–648.
- Kalney E, Kanamitsu M, Kistler R *et al.* (1996) The NCEP/NCAR 40-year reanalysis project. *Bulletin of the American Meteorological Society*, **77**, 437–471.
- Kaminski T, Knorr W, Rayner PJ *et al.* (2002) Assimilating atmospheric data into a terrestrial biosphere model: a case study of the seasonal cycle. *Global Biogeochemical Cycles*, **16**, 1066, doi: 10.1029/2001GB001463.
- Keeling CD, Whorf TP, Wahlen M *et al.* (1995) Interannual extremes in the rate of rise of atmospheric carbon dioxide since 1980. *Nature*, **375**, 666–670.
- Knorr W, Kattge J (2005) Inversion of terrestrial ecosystem model parameter values against eddy covariance measure-

- ments by Monte Carlo sampling. *Global Change Biology*, **11**, 1333–1351.
- Krinner G, Viovy N, de Noblet-Ducoudré N *et al.* (2005) A dynamic global vegetation model for studies of the coupled atmosphere–biosphere system. *Global Biogeochemical Cycles*, **19**, GB1015, doi: 10.1029/2003GB002199.
- Kruijt B, Elbers JA, von Randow C *et al.* (2004) The robustness of eddy correlation fluxes for Amazon rain forest conditions. *Ecological Applications*, **14**, S101–S113.
- Kull O, Kruijt B (1998) Leaf photosynthetic light response: a mechanistic model for scaling photosynthesis to leaves and canopies. *Functional Ecology*, **12**, 767–777.
- Law BE, Falge E, Gu L *et al.* (2002) Environmental controls over carbon dioxide and water vapour exchange of terrestrial vegetation. *Agricultural and Forest Meteorology*, **113**, 97–120.
- Malhi Y, Nobre AD, Grace J *et al.* (1998) Carbon dioxide transfer over a Central Amazonian rain forest. *Journal of Geophysical Research*, **103**, 31593–31612.
- Malhi Y, Pegoraro E, Nobre AD *et al.* (2002) Energy and water dynamics of a central Amazonian rain forest. *Journal of Geophysical Research*, **107**, 45-1–45-17, doi: 10.1029/2001JD000623.
- Miller SD, Goulden ML, Menton MC *et al.* (2004) Biometric and micrometeorological measurements of tropical forest carbon balance. *Ecological Applications*, **14**, S114–S126.
- Moncrieff JB, Malhi Y, Leuning R (1996) The propagation of errors in long-term measurements of land-atmosphere fluxes of carbon and water. *Global Change Biology*, **2**, 231–240.
- Monteith JL (1972) Solar radiation and productivity in tropical ecosystems. *Journal of Applied Ecology*, **9**, 747–766.
- Nabuurs G-J, Schelhaas M-J, Mohren GMJ *et al.* (2003) Temporal evolution of the European forest sector carbon sink from 1950 to 1999. *Global Change Biology*, **9**, 152–160.
- Nemani RR, Keeling CD, Hashimoto H *et al.* (2003) Climate-driven increases in global terrestrial net primary production from 1982 to 1999. *Science*, **300**, 1560–1563.
- New M, Hulme M, Jones P (1999) Representing twentieth-century space-time climate variability. Part I: Development of a 1961–90 mean monthly terrestrial climatology. *Journal of Climate*, **12**, 829–856.
- Olivier JGJ, Berdowski JJM (2001) Global emissions sources and sinks. In: *The Climate System* (eds Berdowski J, Guicherit R, Heij BJ), pp. 33–78. A. A. Balkema Publishers/Swets & Zeitlinger Publishers, Lisse, the Netherlands.
- Papale D, Valentini R (2003) A new assessment of European forests carbon exchanges by eddy fluxes and artificial neural network spatialization. *Global Change Biology*, **9**, 525–535.
- Peylin P, Bousquet P, Le Quéré C *et al.* (2005) Multiple constraints on regional CO<sub>2</sub> flux variations over land and oceans. *Global Biogeochemical Cycles*, **19**, 1–21, doi: 10.1029/2003GB002214.
- Phillips OL, Malhi Y, Higuchi N *et al.* (1998) Changes in the carbon balance of tropical forests: evidence from long-term plots. *Science*, **282**, 439–442.
- Porté A, Loustau D (1998) Variability of the photosynthetic characteristics of mature needles within the crown of a 25-year-old *Pinus pinaster*. *Tree Physiology*, **18**, 223–232.
- Prentice IC, Farquhar GD, Fasham MJR *et al.* (2001) The carbon cycle and atmospheric carbon dioxide. In: *Climate Change 2001: the Scientific Basis. Contribution of Working Group I to the Third Assessment Report of the Intergovernmental Panel on Climate Change* (eds Houghton JT, Ding Y *et al.*), pp. 183–237. Cambridge University Press, Cambridge.
- Press WH, Teukolsky SA, Vetterling WT *et al.* (1992) *Numerical Recipes in Fortran: The Art of Scientific Computing*. Cambridge University Press, Cambridge.
- Raich JW, Schlesinger WH (1992) The global carbon dioxide flux in soil respiration and its relationship to vegetation and climate. *Tellus B*, **44**, 81–99.
- Raupach MR, Rayner PJ, Barrett DJ *et al.* (2005) Model-data synthesis in terrestrial carbon observation: methods, data requirements and data uncertainty specifications. *Global Change Biology*, **11**, 378–397.
- Rayner PJ, Enting IG, Francey RJ *et al.* (1999) Reconstructing the recent carbon cycle from atmospheric CO<sub>2</sub>, δ<sup>13</sup>C and O<sub>2</sub>/N<sub>2</sub> observations. *Tellus B*, **51**, 213–232.
- Rayner NA, Parker DE, Horton EB *et al.* (2003) Global analyses of sea surface temperature, sea ice, and night marine air temperature since the late nineteenth century. *Journal of Geophysical Research*, **108**, 4407, doi: 10.1029/2002JD002670.
- Rayner PJ, Scholze M, Knorr W *et al.* (2005) Two decades of terrestrial carbon fluxes from a carbon cycle data assimilation system (CCDAS). *Global Biogeochemical Cycles*, **19**, 1–20, doi: 10.1029/2004GB002254.
- Reich PB, Walters MB, Kloeppel BD *et al.* (1995) Different photosynthesis-nitrogen relations in deciduous hardwood and evergreen coniferous tree species. *Oecologia*, **104**, 24–30.
- Reichstein M, Tenhunen J, Rouspard O *et al.* (2003) Inverse modelling of seasonal drought effects on canopy CO<sub>2</sub>/H<sub>2</sub>O exchange in three Mediterranean ecosystems. *Journal of Geophysical Research*, **108**, 4726, doi: 10.1029/2003JD003430.
- Robock A (2005) Cooling following large volcanic eruptions corrected for the effect of diffuse radiation on tree rings. *Geophysical Research Letters*, **32**, L06702, doi: 10.1029/2004GL022116.
- Rödenbeck C, Houweling S, Gloor M *et al.* (2003) CO<sub>2</sub> flux history 1982–2001 inferred from atmospheric data using a global inversion of atmospheric transport. *Atmospheric Chemistry and Physics*, **3**, 1919–1964.
- Rosenzweig C, Abramopoulos F (1997) Land-surface model development for the GISS GCM. *Journal of Climate*, **10**, 2040–2054.
- Running SW, Nemani RR, Heinsch FA *et al.* (2004) A continuous satellite-derived measure of global terrestrial primary production. *Bioscience*, **54**, 547–560.
- Running SW, Thornton PE, Nemani RR *et al.* (2000) Global terrestrial gross and net primary productivity from the earth observing system. In: *Methods in Ecosystem Science* (eds Sala O, Jackson R, Mooney H), pp. 44–57. Springer-Verlag, New York.
- Schimel DS, House JI, Hibbard KA *et al.* (2001) Recent patterns and mechanisms of carbon exchange by terrestrial ecosystems. *Nature*, **414**, 169–172.
- Schmidt GA, Ruedy R, Hansen JE *et al.* (2006) Present 6-day atmospheric simulations using GISS ModelE: Comparison to in-situ, satellite, and reanalysis data. *Journal of Climate*, **19**, 153–192.

- Schulz K, Jarvis A, Bevan K *et al.* (2001) The predictive uncertainty of land surface fluxes in response to increasing ambient carbon dioxide. *Journal of Climate*, **14**, 2551–2562.
- Sellers PJ (1987) Canopy reflectance, photosynthesis, and transpiration, II: the role of biophysics in the linearity of their interdependence. *Remote Sensing of Environment*, **21**, 143–183.
- Sitch S, Prentice I, Smith B *et al.* (2000) LPJ – a coupled model of vegetation dynamics and the terrestrial carbon cycle. In: *The role of vegetation dynamics in the control of atmospheric CO<sub>2</sub> content* (Sitch S, PhD thesis). Lund University, Lund, Sweden.
- Sitch S, Smith B, Prentice IC *et al.* (2003) Evaluation of ecosystem dynamics, plant geography and terrestrial carbon cycling in the LPJ dynamic global vegetation model. *Global Change Biology*, **9**, 161–185.
- Takashi T, Wanninkhof RH, Feely RA *et al.* (1999) Net sea-air CO<sub>2</sub> flux over the global oceans: An improved estimate based on the sea-air pCO<sub>2</sub> difference. *Proceedings 2nd CO<sub>2</sub> in Oceans Symposium*, Tsukuba, Japan.
- Tarantola A (1987) *Inverse Problem Theory: Methods for Data Fitting and Parameter Estimation*. Elsevier, Amsterdam.
- Valentini R, Matteucci G, Dolman AJ *et al.* (2000) Respiration as the main determinant of carbon balance in European forests. *Nature*, **404**, 861–865.
- Wang Y-P, Leuning R, Cleugh HA *et al.* (2001) Parameter estimation in surface exchange models using nonlinear inversion: how many parameters can we estimate and which measurements are most useful? *Global Change Biology*, **7**, 495–510.
- White MA, Thornton PE, Running SW *et al.* (2000) Parameterization and sensitivity analysis of the BIOME-BGC terrestrial ecosystem model: net primary production controls. *Earth Interactions*, **4**, 11–85.
- Wilson K, Goldstein A, Falge E *et al.* (2002) Energy balance closure at FLUXNET sites. *Agricultural and Forest Meteorology*, **113**, 223–243.
- Wofsy SC, Goulden ML, Munger JW (1993) Net exchange of CO<sub>2</sub> in a mid-latitude forest. *Science*, **260**, 1314–1317.
- Woodward FI, Lomas MR (2004) Vegetation dynamics – simulating responses to climatic change. *Biological Reviews*, **79**, 643–670.
- Woodward FI, Smith TM, Emanuel WR (1995) A global land primary productivity and phytogeography model. *Global Biogeochemical Cycles*, **9**, 471–490.
- Zaehle S, Sitch S, Prentice IC *et al.* (2006) The importance of age-related decline of forest NPP for modeling regional carbon balances. *Ecological Applications*, **16**.
- Zaehle S, Sitch S, Smith B *et al.* (2005) Effects of parameter uncertainties on the modeling of terrestrial biosphere dynamics. *Global Biogeochemical Cycles*, **19**, GB3020, doi: 10.1029/2004GB002395.